



Research article

Exploring the effective compounds and potential mechanisms of Shengxian Decoction against coronary heart disease by UPLC-Q-TOF/MS and network pharmacology analysis

Hao-ming Zhou^a, Shi-jun Yue^{a,d,*}, Wen-xiao Wang^{a,d}, Qiao Zhang^a, Ding-qiao Xu^a,
Jia-jia Li^a, Yu-ping Tang^{a,**}, Xin-yu Yang^{b,c,***}

^a Key Laboratory of Shaanxi Administration of Traditional Chinese Medicine for TCM Compatibility, and State Key Laboratory of Research & Development of Characteristic Qin Medicine Resources (Cultivation), and Shaanxi Key Laboratory of Chinese Medicine Fundamentals and New Drugs Research, and Shaanxi Collaborative Innovation Center of Chinese Medicinal Resources Industrialization, Shaanxi University of Chinese Medicine, Xi'an, 712046, Shaanxi Province, China

^b Department of Pharmacy, Beijing Shijitan Hospital, Capital Medical University, Beijing, 100038, China

^c Beijing Key Laboratory of Bio-characteristic Profiling for Evaluation of Rational Drug Use, Beijing, 100038, China

^d International Joint Research Center on Resource Utilization and Quality Evaluation of Traditional Chinese Medicine of Hebei Province, Hebei University of Chinese Medicine, Shijiazhuang, 050200, China

ARTICLE INFO

Keywords:

Coronary heart disease
Shengxian Decoction
UPLC-Q-TOF/MS
Network pharmacology
Inflammation
Apoptosis

ABSTRACT

As a well-known classical Chinese medicine prescription, Shengxian Decoction (SXD) has been applied for a century to treat cardiovascular diseases, especially coronary heart disease (CHD), but the potentially effective compounds and underlying mechanisms remain unclear. With ultra-performance liquid chromatography-quadrupole-time of flight-mass spectrometry (UPLC-Q-TOF/MS) and network pharmacology analysis, the potential effective compounds of SXD and their pharmacological mechanisms against CHD were identified and revealed. 57 effective compounds with favorable pharmacokinetic characteristics and biological activities were screened through UPLC-Q-TOF/MS analysis, database and literature mining, interacting with 96 CHD-related targets to support potential synergistic therapeutic actions. Systematic analysis of the PPI network and microarray data further revealed six core targets, including TNF, IL-1 β , IL-6, TP53, VEGFA and PTGS2, which were mainly involved in fluid shear stress and atherosclerosis, lipid and atherosclerosis, PI3K-Akt signaling pathway et al. Moreover, the proposed contribution indexes of effective compounds indicated these compounds, including isoferulic acid, quercetin, calycosin, ferulic acid, kaempferol, calycosin 7-O-glycoside, formononetin, astragaloside IV and saikosaponin D, as the core compounds of SXD. The molecular docking results confirmed that those core compound-target pairs exhibited strong binding energy. Furthermore, we validated that SXD significantly alleviated myocardial tissue injury in CHD rats and reversed H/R-induced decreases in H9c2 cell viability by attenuating the production of TNF, IL-6 and IL-1 β , and reducing

* Corresponding author. Key Laboratory of Shaanxi Administration of Traditional Chinese Medicine for TCM Compatibility, and State Key Laboratory of Research & Development of Characteristic Qin Medicine Resources (Cultivation), and Shaanxi Key Laboratory of Chinese Medicine Fundamentals and New Drugs Research, and Shaanxi Collaborative Innovation Center of Chinese Medicinal Resources Industrialization, Shaanxi University of Chinese Medicine, Xi'an, 712046, Shaanxi Province, China.

** Corresponding author.

*** Corresponding author. Department of Pharmacy, Beijing Shijitan Hospital, Capital Medical University, Beijing, 100038, China.

E-mail addresses: shijun_yue@163.com (S.-j. Yue), yupingtang@sntcm.edu.cn (Y.-p. Tang), yangxinyu@bjsjth.cn (X.-y. Yang).

<https://doi.org/10.1016/j.heliyon.2024.e29558>

Received 21 September 2023; Received in revised form 8 April 2024; Accepted 10 April 2024

Available online 16 April 2024

2405-8440/© 2024 The Authors. Published by Elsevier Ltd. This is an open access article under the CC BY-NC license (<http://creativecommons.org/licenses/by-nc/4.0/>).

cardiomyocyte apoptosis via down-regulating the TP53, caspase3 and cytochrome C mRNA expression levels as well as caspase3, caspase9 and cytochrome C protein expression levels according to RT-qPCR and Western blot results. Our findings explained the pharmacological mechanisms underlying the effectiveness of SXD in the treatment of CHD, and laid a foundation for future basic and clinical research of SXD.

1. Background

Coronary heart disease (CHD) is one of the most common cardiovascular diseases, which is caused by stenosis, spasm or blockage of the coronary artery lumen, and leads to myocardial ischemia, hypoxia or necrosis [1,2]. Chronic ischemia from coronary artery stenosis or rupture and myocardial infarction can lead to heart failure and even death [3]. Drugs for treating CHD usually act on individual targets, such as beta-blockers and angiotensin converting enzyme inhibitors. The current clinical drugs for CHD have good efficacy, but may produce inevitable side effects and drug resistance [4]. In addition, the morbidity and mortality of CHD are on the rise, and gradually show a younger trend. It is particularly important to seek a more effective and safe way to combat CHD.

CHD belongs to the category of “chest arthralgia” in traditional Chinese medicine (TCM), and is characterized by blood stasis, “qi” stagnation (vital energy retardation), and phlegm obstruction [5]. In TCM theory, the “qi” stagnation is deemed as the main pathogenesis of CHD [6]. Shengxian Decoction (SXD), a classic TCM prescription for the treatment of atmospheric subsidence syndrome, was first recorded in the text “Medical Treatise on the Integration of Chinese and Western Medicine” by the famous Chinese medicine master Zhang Xi-chun in the late Qing Dynasty and the early Republic of China (between the 19th and 20th centuries). SXD is composed of HuangQi (HQ, roots of *Astragalus membranaceus* var. *mongholicus* (Bunge) Hsiao), ZhiMu (ZM, rhizomes of *Anemarrhena asphodeloides* Bge.), ChaiHu (CH, roots of *Bupleurum chinense* DC.), JieGeng (JG, roots of *Platycodon grandiflorum* (Jacq.) A. DC.) and ShengMa (SM, rhizomes of *Cimicifuga foetida* L.) at a ratio of 6:3:1.5:1.5:1 [7,8]. In this prescription, HQ is the emperor, which can play the role of replenishing and raising “qi”; as the ministers, CH and SM play a supporting and harmonizing role; the HQ’s medicinal properties are slightly hotter, so ZM plays the role of heat-clearing as the adjuvant herb; JG, as a courier role, can help to guide the other herbs in the formula to the heart and also modulate or harmonize the properties of other drugs. Together, these herbs are particularly effective in treating conditions such as “qi” stagnation, which can manifest as chest tightness, shortness of breath, fatigue, and other symptoms similar to those of CHD [9]. And the main compounds of SXD are flavonoids, phenolic acids, polysaccharides, saponins and amino acids, which are closely related to regulating inflammatory factors, oxidoreductases, and cardiovascular indicators, etc. Based on a metabolomic study, SXD has a cardioprotective effect against chronic heart failure, which is involved in the metabolism of energy and sphingolipid [7]. SXD, in particular, has been clinically used in China to cure a variety of heart diseases, including chronic heart failure and myocardial ischemia, especially CHD [10,11]. However, the potential pharmacological mechanism of SXD in the treatment of CHD, as well as the potential targets and pathways are still unclear.

TCM has the multi-compound, multi-target and multi-pathway characteristics, thus it also belongs to polypharmacy therapy [12]. In recent years, due to the complex composition of TCM prescription, accurate and complete characterization of the prescription is the core problem of TCM research. The ultra-performance liquid chromatography-quadrupole-time of flight-mass spectrometry (UPLC-Q-TOF/MS) is a modern analytical technique to analyze and identify the chemical composition of TCM prescription, which is characterized by rapid and effective qualitative analysis of complex compounds. Besides, network pharmacology can comprehensively and systematically reveal the complex relationship between the effective compounds of TCM and their mechanism of action [13]. It has been successfully applied to interpret the mechanism of the prescription therapy for cardiovascular disease at the molecular network level, such as *Radix Salviae* and Buyang Huanwu Decoction [14,15]. In the present study, we first analyzed the compounds of SXD by UPLC-Q-TOF/MS, and based on which the potential compounds and targets for the treatment of CHD were collected by database and literature analysis. Then, we tried to establish network pharmacology models including protein-protein interaction (PPI), compound-target-disease (C-T-D), and target-pathway (T-P) networks, calculate contribution index (CI) of each effective compound, which was based on chemical, pharmacokinetic and pharmacological data, explore the interaction between compound-target pairs by molecular docking, and construct the rat CHD model and hypoxia/reoxygenation (H/R)-induced H9c2 cell model for further validation, so as to uncover the underlying mechanism of SXD in the treatment of CHD.

2. Methods

2.1. Preparation and analysis of SXD

2.1.1. Preparation of the SXD extract

SXD was prepared as follows: roots of *Astragalus membranaceus* var. *mongholicus* (Bunge) Hsiao (HQ, Batch No. 20220502), rhizomes of *Anemarrhena asphodeloides* Bge. (ZM, Batch No. 20221201), roots of *Bupleurum chinense* DC. (CH, Batch No. 20221101), rhizomes of *Cimicifuga foetida* L. (SM, Batch No. 20221001), and roots of *Platycodon grandiflorum* (Jacq.) A. DC. (JG, Batch No. 20230201) were purchased from Shaanxi Sciendan Pharmaceutical Co., Ltd. (Tongchuan, China) and identified by Professor Yonggang Yan. The voucher specimens were deposited at the Key Laboratory of Shaanxi Administration of Traditional Chinese Medicine for TCM Compatibility, Shaanxi University of Chinese Medicine (Specimen number: 22-05-02, 22-12-01, 22-11-01, 22-10-01, 23-02-01). Seventeen reference standards including mangiferin (Batch No. Yz111920), caffeic acid (Batch No. Yz012423), rutin (Batch No.

Yz051924), Calycosin 7-O-glucoside (Batch No. Yz102721), ferulic acid (Batch No. Yz011422), isoferulic acid (Batch No. Yz1009201), luteolin (Batch No. 116523), quercetin (Batch No. Yz011823), calycosin (Batch No. Yz120322), kaempferol (Batch No. Yz110987), isorhamnetin (Batch No. Yz090422), saikosaponin A (Batch No. Yz050723), astragaloside IV (Batch No. Yz081320), saikosaponin D (Batch No. Yz080522), neomangiferin (Batch No. Yz1027222), timosaponin AIII (Batch No. Yz111022) and timosaponin BII (Batch No. Yz072323) were obtained from Nanjing Plant Origin Biological Co., Ltd. (Nanjing, China).

SXD water extraction solution was prepared as follows: the slices of HQ (22.38 g), CH (5.60 g), JG (5.60 g) and SM (3.73 g) were evenly mixed, added 10 times water (MILLI-Q IQ 7000, MA, USA) was added, soaked for 30 min, ZM (11.19 g) was added after boiling for 8 min, and boiled for another 7 min, and then strained. Next, the residue was added with 8 times the amount of water, boiled for 10 min, and filtrate was mixed twice [16]. The water extraction was filtered with gauze, and freeze-dried to obtain SXD freeze-dried extract (Labconco Freezone 4.5L, MO, USA) The SXD freeze-dried extract was diluted with water to a certain concentration, and then used for subsequent experiments.

SXD ethanol extraction solution was prepared as follows: HQ (22.38 g), ZM (11.19 g), CH (5.60 g), JG (5.60 g) and SM (3.73 g) were immersed in 485 mL of 70 % ethanol solution for 1 h and refluxed three times for 1 h each [17]. The combined ethanol extraction was filtered by a 0.22 μm filter, and then diluted to 1 mg/mL for chemical fingerprint analysis.

2.1.2. Chemical fingerprint of SXD by ultra-performance liquid chromatography-quadrupole-time of flight-mass spectrometry (UPLC-Q-TOF/MS)

The chemical fingerprint of SXD was determined by UPLC-Q-TOF/MS. The concentration of SXD water and ethanol extraction solution was 1 mg/mL, filtered by 0.22 μm filter, and injected into UPLC-Q-TOF/MS for analysis. The samples were analyzed by Waters Acquity SDS system. The mobile phases of UPLC were 0.1 % formic acid and acetonitrile on a ACQUITY UPLC HSS T3 column (2.1 mm \times 100 mm, 1.8 μm) at a flow rate of 0.3 mL/min. Optimized gradient elution was as follows: 0–2 min, 10%–35 % acetonitrile; 2–15 min, 35%–95 % acetonitrile; 15–17 min, 95 % acetonitrile; 17–18 min, 95%–10 % acetonitrile; 18–20 min, 10 % acetonitrile. Column temperature was maintained at 35 $^{\circ}\text{C}$.

The relevant parameters of MS were set as follows: positive ion mode analysis, capillary voltage of 3.0 kV, source temperature of 100 $^{\circ}\text{C}$, desolvent temperature of 350 $^{\circ}\text{C}$, cone-hole gas flow of 50 L/h, nitrogen as atomizing gas (600 L/h), scanning mode of full scan, scanning range m/z 50–1200 Da; negative ion mode analysis, capillary voltage of 2.5 kV, source temperature of 100 $^{\circ}\text{C}$, desolvent temperature of 280 $^{\circ}\text{C}$, cone-hole gas flow of 50 L/h, nitrogen as atomizing gas (600 L/h), scanning mode of full scan, scanning range m/z 50–1200 Da. Data was collected and analyzed using MassLynx V4.2 software (Waters, USA).

2.2. Network pharmacology

2.2.1. Screening the effective compounds and predicting the potential targets of SXD

The compounds of SXD were collected from multiple sources, including the compounds by UPLC-Q-TOF/MS, the Traditional Chinese Medicine System Pharmacology Database and Analysis Platform (TCMSP, <https://tcmspe.com/>), and literature mining. The compounds were collected using “Huangqi”, “Zhimu”, “Chaihu”, “Shengma” and “Jiegeng” as search terms in TCMSP [18]. These compounds were screened by oral bioavailability (OB) \geq 30 % and drug-likeness (DL) \geq 0.18, and their PubChem ID (<https://pubchem.ncbi.nlm.nih.gov/>) were recorded. OB represents the oral availability of pharmaceutical compounds, and DL refers to the similarity between compound and a known drug [19]. At the same time, the effective compounds of SXD were imported into TCMSP database to obtain targets. The compounds with fewer targets were imported into the PubChem database to obtain their Canonical SMILES numbers and then imported into the Swiss Target Prediction database (<http://www.swisstargetprediction.ch/>) to predict the possible targets. All targets were integrated and entered the UniProt database (<https://www.uniprot.org/>) for verification, and duplicated targets were deleted to obtain the SXD-related targets.

2.2.2. Seeking out the potential targets of SXD in the treatment of CHD

With “coronary heart disease” as the keyword, GeneCards Database (<https://www.genecards.org/>), Online Mendelian Inheritance in Man Database (<https://www.omim.org/>), Therapeutic Target Database (<http://db.idrblab.net/ttd/>) and DisGeNET Database (<https://www.disgenet.org/search>) were used to search and screen the known CHD-related targets, and the repeated targets in the search results were discarded. However, there were too many results in those databases, so targets with a target score greater than 50 in the GeneCards database and a Score greater than 0.1 in the DisGeNET database were reserved. The UniProt knowledge base was used to get the standard target’s name with the organism selected as “*Homo sapiens*”. Finally, the potential targets of SXD acting on CHD were obtained by using the Venny 2.1.0 platform (<https://bioinfo.cnb.csic.es/tools/venny/index.html>).

2.2.3. Construction and analysis of the protein-protein interaction (PPI) network

These potential targets were imported into the STRING database (<https://string-db.org/>) to construct the PPI network. The organism was set to “*Homo sapiens*” and the minimum required interaction score was “medium confidence (0.4)”, and then the PPI network was constructed. Subsequently, the PPI network was saved in “tsv” file format, which was imported into Cytoscape 3.8.2 software (<https://cytoscape.org/>), an open-source software package project, to analyze the results by the network topology analysis function. In the PPI network, the degree value is an important index, and these targets above the average value usually play an important role. So, we ranked these targets according to degree value. At the same time, the important potential targets were screened out according to the average of degree and betweenness centrality of the node. Then, the target sub-networks were identified from the PPI network by using the MCODE plugin. Finally, the overlapping of the core sub-networks cluster and important potential targets was

taken as the key targets.

Furthermore, we analyzed the PPI network obtained with the CytoHubba plugin. Four target-ranking methods, including Edge Percolated Component, Eccentricity, Closeness, and Radiality, were used to analyze targets' weight (S-value) [20]. Each method allowed the targets to receive a score, and then we ranked the targets according to the score. Targets with higher scores were ranked higher. For example, the highest scoring target was ranked first. However, many targets contained the same score, and it didn't matter how many targets contained the same score, the rank of the next target increased by one. Subsequently, all potential targets were ranked according to these four methods. If the rank of each target exceeded its median rank, the S-value of this target was increased by 1. Therefore, the maximum S-value of each target was 4 and the minimum was 0. Finally, we analyzed the targets' weight according to the S-value of targets for subsequent analysis.

2.2.4. Microarray data analysis of core targets

Since myocardial infarction (MI) is one of the most serious and harmful diseases in CHD, the published microarray data (accession number GSE66360) of circulating endothelial cells of patients with MI and control were searched through the GEO database to characterize the significance of key targets (<https://www.ncbi.nlm.nih.gov/geo>). The gene expression profile dataset GSE66360 comprised the gene expression data of circulating endothelial cells samples from 50 healthy donors and 49 patients with MI. This data was based on the GPL570 Affymetrix Human Genome U133 Plus 2.0 array. For the expression profile dataset, we first obtained the annotation information of the probes according to the corresponding platform, mapped the probes to genes, removed multiple matches, used the mean value as the gene expression when multiple probes matched to a gene, and finally obtained the gene expression profile. The RStudio software's Limma package was used for the identification of the differences in expression level of key targets between control and patients with MI. The cutoff criteria in this analysis were set as $p < 0.05$ and $|\log FC| > 1$. The key targets of expression difference were regarded as the core target of SxD in the treatment of CHD.

2.2.5. Construction of the compound-target-disease (C-T-D) network

The effective compounds and their potential targets in SxD were made into qualified target table and type table, and imported into Cytoscape 3.8.2 software for visualizing and analyzing the interaction networks. Subsequently, a C-T-D network was constructed, while the size and color depth of the potential targets were adjusted according to the degree value. Finally, we analyzed the parameter rank-sum ratio (RSR) of this network, which was calculated from network topology parameters, including Betweenness, Closeness, Degree, Eccentricity, Neighborhood Connectivity and Average Shortest Path Length.

2.2.6. Contribution index (CI) calculation

In order to screen the core compounds of SxD acting on CHD, a CI based on the intrinsic properties (content) of the effective compound in the corresponding herb and the importance of the effective compound in the C-T-D network was calculated [21,22]. The analysis was organized as follows:

$$W_j = \frac{\sum_i^N S_i}{N}$$

$$CI_j = \frac{m_i}{\sum_i^n m_i} \times \frac{C_{ij}}{M_j} \times OB_j \times RSR_j \times W_j \times 10^7$$

where S_i is the S-value of the potential target i ; N is the number of potential targets acted by compound j ; W_j is the average S-value of all potential targets acted by compound j ; m_i is the weight of herb i in SxD; n is the total count of herbs in SxD; $\frac{m_i}{\sum_i^n m_i}$ is the proportion of each herb in SxD (a common compound is the sum of the proportions of the herbs, which belongs in these herbs); C_{ij} is the content of the compound j in herb i (the content of effective compounds was collected by literature mining, which was expressed as the average content reported in the literature); M_j is the molecular weight of the compound j ; $\frac{C_{ij}}{M_j}$ represents the molar concentration of 1 g of the compound in SxD; OB_j is the oral bioavailability of compound j ; RSR_j is the rank-sum ratio of the integrated network topology parameters of the compound j in the C-T-D network. This method was used to reflect the ratio of the compounds in SxD and the weight efficiency of their effect on potential CHD-related targets. Thus, a compound with a higher CI means a higher probability of the effect on CHD.

2.2.7. Gene ontology (GO) and Kyoto Encyclopedia of genes and genomes (KEGG) enrichment analysis and target-pathway (T-P) network construction

The potential targets were imported into the DAVID platform (<https://david.ncifcrf.gov/tools.jsp>) for GO function enrichment analysis and KEGG pathway enrichment analysis, and the "select species" was set to "Homo sapiens". GO enrichment analysis involved the biological process (BP), cellular component (CC) and molecular function (MF) of the potential targets, and the top 10 results were visualized as bar graphs. Based on the S-values of all potential targets, the weight of the pathway P was the sum of the corresponding targets. Pathway analysis was performed with KEGG, and the top 20 results were visualized as a bubble diagram by using bioinformatics platform (<http://www.bioinformatics.com.cn/>). Subsequently, the T-P network was constructed by Cytoscape 3.8.2 software according to the top 20 of P-weight [23].

2.2.8. Molecular docking

First, we downloaded the 3D structures of the core compounds in SxD from the PubChem database and saved them in “sdf” format, and then downloaded the 3D structures of the core targets from the PDB database (<https://www.rcsb.org/>) and saved them in “pdb” format. We would use Chem 3D software to construct their 3D structures for some compounds, which did not have 3D structures in the database. These compounds and targets were prepared for ligands and receptors by using AutoDockTools software, which included operations such as dehydration, hydrogenation, and deionization. These compound-target pairs were then docked, and the docking scores were made into a heat map. Finally, the lower binding energy docking results of each core target were visualized by LigPlot (<https://www.ebi.ac.uk/thornton-srv/software/LigPlus/>) and PyMOL (<https://pymol.org/2/>) software.

2.3. In vivo experiments

2.3.1. Experimental animals

Male specific pathogen-free Sprague-Dawley rats (180–200 g) were purchased from the Beijing Vital River Laboratory Animal Technology Co Ltd (Beijing, China). All experimentals were conducted according to the Guide for the Care and Use of Laboratory Animals by the National Institute of Health (USA). All procedures were strictly approved by the Animal Experiment Ethics Committee of the Shaanxi University of Chinese Medicine (Ethics Approval No. SUCMDL20220310006). All rats were housed under the standard conditions (temperature, 25 ± 2 °C; constant humidity, 55 ± 5 %; 12 h dark/light cycle; freely available food and purified water).

After one week of adaptive feeding, all rats were randomly selected for sham surgery or CHD model group. The rat CHD model was established by exhaustive swimming, restricted diet and ligation of the left anterior descending coronary artery. The rats in sham surgery group were fed normally. On the first day of the experiment, the rats in the CHD model group swam exhaustively once a day, with the standard of exhaustively swimming being that the head of the rats could not emerge from the water level for 10 s. At the same time, the food control was carried out, and the daily intake was half of the normal diet for 21 days. On day 22 of the experiment, a left thoracotomy was performed after rats were anesthetized with 2 % isoflurane. The rats were laid flat and disinfected, and incised from the front skin of the neck to extract tissue and muscle, exposing the windpipe, which was then inserted into the oral cavity and connected to a ventilator. The left third and fourth intercostal spaces of the rat were then propped open with hemostatic forceps, and the left anterior descending coronary artery (LAD) was then ligated with a 6-0 surgical sutures. After the ligation, the heart was placed back in the chest cavity, the air that entered the chest cavity was expelled, the chest cavity was closed, and the skin was sutured. 0.25 mL penicillin was injected immediately after chest closure. For the sham-operated group, rat LADs were only threaded and not ligated, and the remaining procedures were the same as those in the CHD group [24]. All rats were fed normally after modeling. The 24 CHD-operated rats were divided into the CHD model group, the SxD low-dose group (4.33 g/kg), SxD high-dose group (12.99 g/kg), and Betaloc group (10 mg/kg, AstraZeneca, UK) according to a random number control table. Rats without ligation were placed in the sham-operated group. The rats in the sham and CHD model groups were given the same volume of normal saline *via* intragastric administration.

2.3.2. Myocardial infarct size detection

After 28 days of treatment, the rats were given 12 h of fasting and water, 2 % isoflurane for anesthesia, all the hearts of the rats were separated, weighed after absorbing water, and the heart weight index (HWI) was calculated. Three rats in each group were randomly selected and their hearts were transferred at 0–4 °C PBS and frozen at –20 °C for 30 min. Slices of the heart were taken with a thickness of 2 mm and placed in 2 % red tetrazolium solution in a dark water bath at 37 °C for 30 min. The container was slightly shaken every 5 min to make it fully stained. The myocardial sections were removed and washed with PBS solution for 3–5 min. Next, the sections were soaked in 4 % paraformaldehyde solution for 24 h, and the myocardial infarction size was evaluated by 2,3,5-triphenyl-2H-tetrazolium chloride (TTC) staining. Image Pro Plus 6.0 was used to quantify the myocardial infarction size. Myocardial infarction area divided by total area was regarded as the percentage of myocardial infarction.

2.3.3. Hematoxylin and eosin (H&E) and Masson's trichrome staining

The myocardial tissue was fixed in 4 % paraformaldehyde solution, gradient dehydrated with 70–100 % ethanol, embedded in paraffin, and sliced (4–5 μ m). Hematoxylin-eosin (H&E) staining was used to observe myocardial structural changes under an optical microscope. The paraffin sections were dewaxed to water, followed by Masson staining of the sections. After dehydration and sealing, the changes of myocardial collagen fibers were observed under an optical microscope to evaluate the degree of myocardial fibrosis.

2.3.4. ELISA

Blood was collected by intubation in the abdominal aorta of rats in each group, and serum was obtained by centrifugation at 3000 rpm for 15 min. The levels of serum IL-6 (MM-0190R1, MEIMIAN, China), IL-1 β (MM-0047R1, MEIMIAN, China), Aldosterone (ALD, YJ002876, MEIMIAN, China), Angiotensin II (Ang II, YJ058803, MEIMIAN, China), N-terminal pro-brain natriuretic peptide (NT-proBNP, YJ003242, MEIMIAN, China) were assessed at 450 nm was detected by a microplate reader (RT-6100, Rayto, China) according to the ELISA kits.

2.4. In vitro experiments

2.4.1. Cell culture and the hypoxia/reoxygenation (H/R) cell model

Rat cardiomyocytes (H9c2) were normally cultured in Dulbecco's Modified Eagle Medium (DMEM) supplemented with 10 % FBS at

a 37 °C normoxic atmosphere with 5 % CO₂. The DMEM medium containing 10 % FBS was used as a complete medium. An H/R cell model was used to mimic the pathological process of cardiac injury. In brief, the H9c2 cells were in six groups: the control group, H9c2 cells were normally cultured; the H/R group, H9c2 cells were cultured in D-Hank's medium in a hypoxia atmosphere at 37 °C with 5 % CO₂ and 95 % N₂ for 8 h, and further cultured in complete medium at normoxic atmosphere at 37 °C with 5 % CO₂ and 95 % O₂ for 12 h; the H/R + treatment group, H9c2 cells were incubated in an anesthesia induction chamber with fresh gas (95 % O₂ and 5 % CO₂) and the addition of drug (100 μM Diazoxide, 250 μg/mL SXD, 500 μg/mL SXD, 1 mg/mL SXD) for 24 h, and then treated with H/R.

2.4.2. Cell viability assay

3-(4,5)-dimethylthiazazo (-z-y1)-3,5-di- phenyltetrazoliumromide (MTT) assay was used in the current study to evaluate cell viability after various treatments. After the collection of H9c2 cells, 10 μL MTT reagents (5 mg/mL) were added into the 96-well plate (1.0 × 10⁵ cells/1 mL) and then incubated for 4 h. After the solution was discarded, 100 μL of dimethyl sulfoxide was added into the culture plate. Finally, an Imark microplate reader was used for measuring the cell absorbance at 570 nm.

2.4.3. Detection of intracellular reactive oxygen species (ROS) generation

Assessment of intracellular ROS changes in cells during apoptosis was performed using Reactive Oxygen Species Assay Kit (S0033 M, Beyotime, China). A cell density of 10⁵/mL was placed in each 35-mm culture plate. DCFH-DA was diluted in serum-free medium at 1:1000 to give a final concentration of 10 μM/L. Cells were collected and suspended in diluted DCFH-DA at a concentration of 1 million to 20 million cells/mL and incubated in a cell incubator at 37 °C for 20 min. The mixture was reversed every 5 min to make full contact between the probe and the cell. Cells were washed three times with serum-free cell culture medium and then analyzed by the Beckman CytoFlex Sflow cytometer system.

2.4.4. Quantification of cellular apoptosis

The apoptosis of H9c2 cells was detected using Annexin V-FITC/PI stain kit (C1062 M, Beyotime, China). In brief, after the cell collection, the H9c2 cells were washed by PBS twice, centrifuged (500×g) for 5 min, and then mixed with 500 μL working buffer. The cells were further added with 5 μL Annexin V binding with FITC and 5 μL PI for 15 min staining. Lastly, cell signal was measured, and the apoptosis rate was analyzed by the Beckman CytoFlex Sflow cytometer system.

2.4.5. ELISA

H9c2 cells were inoculated in 6-well plates with a density of 1 × 10⁵ cells per well. After the drug intervention, the supernatant was taken, and the optical density of tumor necrosis factor (TNF, FU-D1393, BIOFINE, USA), interleukin-6 (IL-6, FU-D1083, BIOFINE, USA) and interleukin-1 beta (IL-1β, FU-D1032, BIOFINE, USA) at 570 nm was detected by a microplate reader according to the ELISA kits.

2.4.6. Real time quantitative PCR (RT-qPCR)

Total RNA was isolated from H9c2 cells with a RNeasy mini kit as described in the manufacturer's manual. These RNA samples were then reverse transcribed into cDNAs using Revert Ace kit (TOYOBO, Japan) and the mRNAs were measured through the SYBR-Green RT-qPCR. *Cellular tumor antigen p53 (TP53)*, *Caspase 3* and *Cytochrome C* expression was calculated relative to the *β-actin* expression (Table 1).

2.4.7. Western blot analysis

H/R-induced H9c2 cells were treated with SXD, and then the proteins from each treatment group were isolated by radio immunoprecipitation assay buffer (RIPA, P1003B, Beyotime, China). The supernatant was centrifuged at 14,000 rpm for 15 min at 4 °C, and the total protein concentration was determined, followed by quantitation with the bicinchoninic acid assay (BCA) protein assay kit (P0010, Beyotime, China). After denaturation in sodium dodecyl sulfate-polyacrylamide gel electrophoresis (SDS-PAGE) gels, the equal amounts of proteins were transferred to nitrocellulose membrane (HATF00010, Millipore, USA). Blots were blocked with 5 % fat-free milk in TBS with Tween-20 (TBST) at room temperature (approximately 25 °C) for 1 h, and then Caspase3 (1:500, 19677-1-AP, Proteintech, USA), Caspase9 (1:500, bs-20773R, Bioss, Switzerland), Cytochrome C (1:500, bs-0013R, Bioss, Switzerland), *β-actin* (1:5000, 200068-8F10, ZEN-BIOSCIENCE, China) primary antibodies were added in 5 % blocking buffer at 4 °C overnight. After incubation with the corresponding HRP-conjugated secondary antibodies (1:2000, SA00001-1 and SA00001-2, Proteintech, USA), the enhanced chemiluminescence (ECL) kit (WBKLS0500, Millipore, USA) was used for detection. The grey scale values of protein bands were analyzed using Image J software (NIH, USA).

Table 1
Primers sequences used for RT-qPCR.

Genes	Forward primer	Reverse primer	Size (bp)
<i>TP53</i>	AGATGTTCCGAGAGCTGAATGAG	TTTTTTATGGCGGGACGTAGA	130
<i>Caspase3</i>	ACTGGAAGCCGAAACTCTCATCA	GGAAGTCGGCCTCCACTGGTATC	127
<i>Cytochrome C</i>	GCTGGATTCTCTTACACAGATGCC	GGTCTGCCCTTCTCCCTTCTT	151
<i>β-actin</i>	AGAGGAAATCGTGCGTGA	CATTGCCGATAGTGATGACCT	144

2.4.8. Caspase-3 enzymatic activities

The caspase 3 can catalyze substrate acetyl-Asp-Glu-Val-Asp *p*-nitroanilide (Ac-DEVD-pNA) to produce yellow *p*-nitroaniline (pNA), so as to determine the activity of caspase 3 by using the caspase 3 Activity Assay Kit (C1115, Beyotime, China). The protein concentrations were determined by Bradford protein assay kit (P0006, Beyotime, China). Cellular extracts (30 μ g) were incubated in a 96-well microtitre plate with 20 ng Ac-DEVD-pNA for 4 h at 37 °C, and OD_{405nm} values were measured by using a microplate reader (BioTek Instruments, USA).

2.5. Statistical analysis

The study data were analyzed using SPSS 22.0 (SPSS Inc., Chicago, IL, USA) and GraphPad Prism 8.3 software (GraphPad Software, USA), and comparisons between the groups were performed using Student's t-test (two-group comparison) and one-way analysis of variance (ANOVA, more than two groups). All data were based on at least three independent experiments. The statistical results are expressed as the mean \pm standard deviation, and then statistical charts were drawn according to the statistical results. Value of $p < 0.05$ was considered to be statistically significant.

3. Results

3.1. Chemical fingerprint of SXD

MassLynx V4.2 software was used to collect the data, and the obtained data were quickly matched to the database in UNIFI 1.8 (Waters) platform. Before conducting the matching process, we created a compound library in-house by gathering chemical formulas for SXD from various sources such as Chemical Book, PubChem, TCMSP, and relevant literature. The compounds in the SXD ethanol extraction solution produced the $[M + H]^+$, $[M + Na]^+$, $[M + NH_4]^+$ and $[M + K]^+$ peaks in the positive ion mode, and produced the $[M - H]^-$, $[M + CH_3COO]^-$ and $[M + HCOO]^-$ peaks in the negative ion mode. The chemical fingerprint of SXD was profiled by UPLC-Q-TOF/MS (Fig. 1). Meanwhile, we identified 113 compounds in SXD, including flavonoids, organic acids, alkaloids, terpenoids, and saponins. Table 2 lists the retention time, molecular formula, adduction ion and fragment ion of all identified compounds, and these compounds have possible biological activity. Seventeen of them were unambiguously identified by comparison with reference compounds (Fig. S1).

3.2. Collecting and screening of effective compounds and the targets in SXD

In the present study, based on UPLC-Q-TOF/MS analysis and the set conditions in the database, a total of 57 potentially effective compounds were retrieved and screened from chemical fingerprint, TCMSP and literature mining, including 17, 11, 12, 8, 5 and 4 form HQ, ZM, CH, SM, JG and common compounds in SXD (Table 3). Among them, isorhamnetin (M54) was shared in HQ and CH, kaempferol (M55) was shared in HQ, ZM and CH, quercetin (M56) was shared in HQ and CH, and stigmasterol (M57) was shared in ZM, CH and SM. Some compounds that did not meet both the OB and DL criteria were also selected in the cases of high bioactivities and

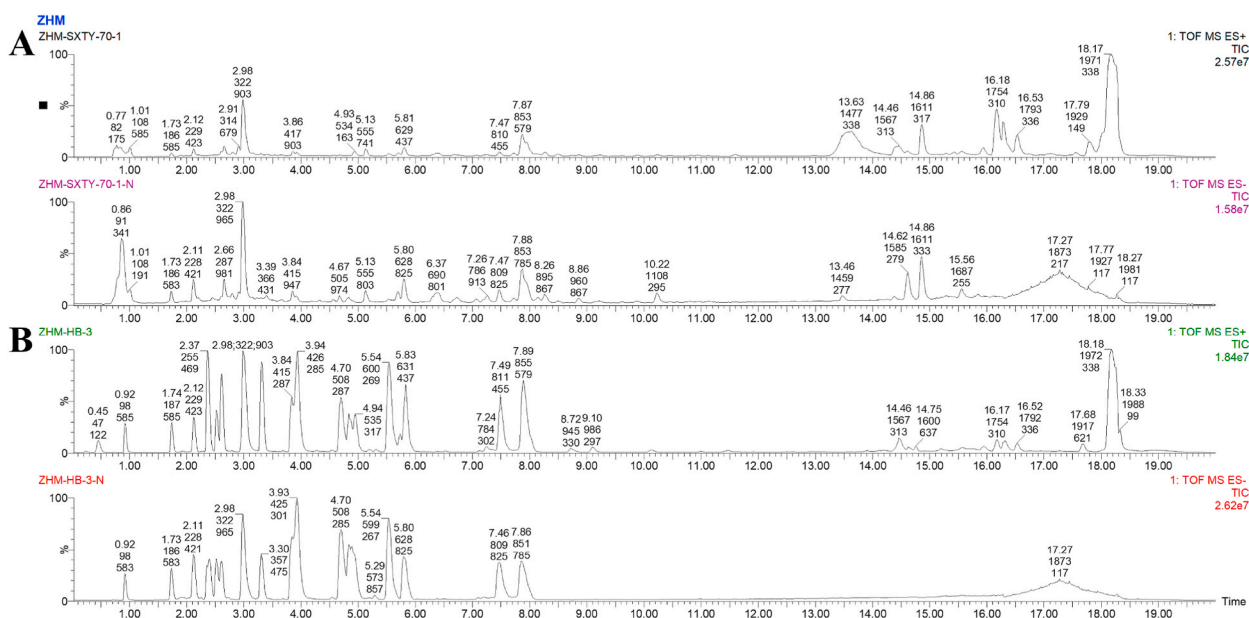


Fig. 1. Base peak ion (BPI) chromatogram of SXD based on UPLC-Q-TOF/MS. (A) Ethanol extraction solution; (B) Reference compounds solution.

Table 2
Identification of chemical compounds in SXD by UPLC-Q-TOF/MS.

No.	Component name	Formula	Neutral mass (Da)	Observed m/z	Mass error (ppm)	Adducts	Observed RT (min)	Fragments (m/z)	Source
1	L(+)-Arginine	C ₆ H ₁₄ N ₄ O ₂	174.1117	173.1041	-1.7	[M - H] ⁻	0.78	131.0821	HQ
2	7-O-Methylmangiferin	C ₂₀ H ₂₀ O ₁₁	436.1005	495.1097	-9.5	[M + CH ₃ COO] ⁻	0.90	435.9157, 351.0805, 245.0365	ZM
3	Ononin	C ₂₂ H ₂₂ O ₉	430.1264	429.1228	8.6	[M - H] ⁻	0.94	431.1304, 269.1013, 224.0434, 118.0476	HQ
4	Nicotinic acid	C ₆ H ₅ NO ₂	123.0320	182.0448	-6.1	[M + CH ₃ COO] ⁻	0.97	-	HQ
5	Boc-D-Tyr-OH	C ₁₄ H ₁₉ NO ₅	281.1263	299.1596	-1.7	[M + NH ₄] ⁺	1.01	265.1544, 250.1418, 235.0709	HQ
6	N-Carbobenzoxy-DL-Leucine	C ₁₄ H ₁₉ NO ₄	265.1314	283.1665	4.5	[M + NH ₄] ⁺	1.35	230.1685, 212.1597	HQ
7	4-Hydroxybenzaldehyde	C ₇ H ₆ O ₂	122.0368	181.0501	-2.7	[M + CH ₃ COO] ⁻	1.46	-	ZM
8	Guaiacol	C ₇ H ₈ O ₂	124.0524	123.0451	-0.3	[M - H] ⁻	1.65	-	SM
9	Neomangiferin ^a	C ₂₅ H ₂₈ O ₁₆	584.1377	583.1161	-	[M - H] ⁻	1.73	301.0249, 272.0245, 243.0229	ZM
10	4-Hydroxy-3,5-dimethoxycinnamic acid	C ₁₁ H ₁₂ O ₅	224.0685	223.0615	1.4	[M - H] ⁻	1.98	223.0618, 135.0454	SM
11	1-Caffeoylquinic acid	C ₁₆ H ₁₈ O ₉	354.0951	353.0878	0.1	[M - H] ⁻	2.04	353.0810, 85.0263	JG
12	Mangiferin ^a	C ₁₉ H ₁₈ O ₁₁	422.3396	421.0559	-	[M - H] ⁻	2.11	301.0249, 271.0113, 258.0078	ZM
13	Cimicifugamide or its isomer	C ₂₅ H ₃₁ NO ₁₀	505.1948	506.2054	6.5	[M+H] ⁺	2.18	344.1657, 177.0851, 145.0580	SM
14	Caffeic acid ^a	C ₉ H ₈ O ₄	180.1574	179.0247	-	[M - H] ⁻	2.4	165.0556, 135.0451, 134.0369	HQ, SM
15	Kaempferol-3-O-Rutinoside	C ₂₇ H ₃₀ O ₁₅	594.1585	593.1511	-0.1	[M - H] ⁻	2.43	285.0423, 239.0477	HQ
16	Rutin ^a	C ₂₇ H ₃₀ O ₁₆	610.5175	609.1237	-	[M - H] ⁻	2.52	300.0175, 271.0113, 243.0161, 227.0225	CH
17	Calycosin 7-O-glucoside ^a	C ₂₂ H ₂₂ O ₁₀	446.4041	491.1012	-	[M + HCOO] ⁻	2.62	283.0540, 268.0344, 239.0275, 211.0333	HQ
18	Naringin	C ₂₇ H ₃₂ O ₁₄	580.1792	639.1935	0.7	[M + CH ₃ COO] ⁻	2.71	433.0741, 271.0401, 151.0402	HQ
19	Isorhamnetin 3,4'-diglucoside	C ₂₈ H ₃₂ O ₁₇	624.1690	623.1613	-0.7	[M - H] ⁻	2.74	541.1690, 342.1341, 301.0348	HQ
20	Tuberosine A	C ₁₉ H ₂₁ NO ₅	343.1420	342.1340	-2.1	[M - H] ⁻	2.76	342.1341, 193.0506	CH
21	Genistin	C ₂₁ H ₂₀ O ₁₀	432.1057	477.1036	-0.6	[M + HCOO] ⁻	2.9	268.0371, 211.0101	HQ
22	Acacetin	C ₁₆ H ₁₂ O ₅	284.0685	283.0608	-1.5	[M - H] ⁻	2.91	226.1017, 212.0438	JG
23	Cimicifugic acid D	C ₂₀ H ₁₈ O ₁₀	418.0900	417.0825	-0.5	[M - H] ⁻	2.93	255.0475, 179.0306	SM
24	Timosaponin D	C ₄₅ H ₇₄ O ₁₉	918.4824	963.4801	-0.6	[M + HCOO] ⁻	2.95	755.4228, 593.1825, 191.0169	ZM
25	Ferulic Acid ^a	C ₁₀ H ₁₀ O ₄	194.1840	193.0453	-	[M - H] ⁻	2.96	178.0206, 134.0313	SM
26	Timosaponin B II ^a	C ₄₅ H ₇₆ O ₁₉	920.4981	965.4958	-0.5	[M + HCOO] ⁻	2.99	919.4790	ZM

(continued on next page)

Table 2 (continued)

No.	Component name	Formula	Neutral mass (Da)	Observed m/z	Mass error (ppm)	Adducts	Observed RT (min)	Fragments (m/z)	Source
27	Isoferulic acid ^a	C ₁₀ H ₁₀ O ₄	194.1840	193.0393	–	[M – H] [–]	3.04	178.0306, 134.0363	SM
28	5-Methyl furfural	C ₆ H ₆ O ₂	110.0368	109.0306	9.6	[M – H] [–]	3.07	108.0217	SM
29	Paeoniflorin	C ₂₃ H ₂₈ O ₁₁	480.1632	519.1229	–6.6	[M+K] ⁺	3.09	449.1431, 327.1342, 165.0415, 121.0984	SM
30	Baicalin	C ₂₁ H ₁₈ O ₁₁	446.0849	445.0781	1	[M – H] [–]	3.15	269.0297, 113.5667	HQ
31	Ethyl 4-hydroxy-3-methoxycinnamate	C ₁₂ H ₁₄ O ₄	222.0892	221.0818	–0.6	[M – H] [–]	3.23	187.0971, 125.0970	SM
32	Cimilactone A	C ₃₃ H ₅₀ O ₉	590.3455	591.3516	–1.9	[M+H] ⁺	3.26	433.3441, 415.3356, 301.0968	SM
33	Desapioplatycodin D	C ₅₂ H ₈₄ O ₂₄	1092.5353	1091.5288	0.7	[M – H] [–]	3.27	1091.5263	JG
34	Puerarin	C ₂₁ H ₂₀ O ₉	416.1107	475.1238	–1.8	[M + CH ₃ COO] [–]	3.31	267.0659, 252.0424, 223. 0388	SM
35	N- <i>p</i> -trans-Coumaroyltyramine	C ₁₇ H ₁₇ NO ₃	283.1208	282.1129	–2.5	[M – H] [–]	3.51	282.1137, 179.0347, 152.9960	ZM
36	Jaranol	C ₁₇ H ₁₄ O ₆	314.0790	373.0926	–0.7	[M + CH ₃ COO] [–]	3.53	299.0926, 282.1137, 179.0347, 152.9960	HQ
37	Methylnissolin-3-O-glucoside	C ₂₃ H ₂₆ O ₁₀	426.1526	507.1503	–1	[M + HCOO] [–]	3.54	483.2362	HQ
38	Platycoside M ₃	C ₅₂ H ₈₀ O ₂₄	1088.5040	1147.5211	2.9	[M + CH ₃ COO] [–]	3.59	933.4736, 653.3382	JG
39	7,2'-dihydroxy-3',4'-dimethoxyisoflavane-7-O-glucoside or its isomer	C ₂₃ H ₂₈ O ₁₀	464.1683	463.1603	–1.4	[M – H] [–]	3.61	353.1018, 301.1079	HQ
40	Isochlorogenic acid C	C ₂₅ H ₂₄ O ₁₂	516.1268	517.1384	8.4	[M+H] ⁺	3.67	451.3312, 269.1081	CH
41	Timosaponin F	C ₃₉ H ₆₄ O ₁₅	772.4245	817.4225	–0.3	[M + HCOO] [–]	3.78	771.4069, 609.2312	ZM
42	Luteolin ^a	C ₁₅ H ₁₀ O ₆	286.2363	285.0276	–	[M – H] [–]	3.84	145.9290	JG
43	Anemarsaponin B	C ₄₅ H ₇₄ O ₁₈	902.4875	947.4865	0.8	[M + HCOO] [–]	3.85	901.4807, 797.4692, 739.4276, 639.3372	ZM
44	Methylnissolin	C ₁₇ H ₁₆ O ₅	300.0998	299.0925	–0.1	[M – H] [–]	3.86	301.0325, 163.3195, 147.0660, 113.7024	HQ
45	Quercetin ^a	C ₁₅ H ₁₀ O ₇	302.2357	301.0249	–	[M – H] [–]	3.91	285.0276, 268.0273	HQ, CH
46	Icariin I	C ₂₇ H ₃₀ O ₁₁	530.1788	569.1412	–1.4	[M+K] ⁺	3.93	451.3323, 258.1019, 270.0794	ZM
47	calycosin ^a	C ₁₆ H ₁₂ O ₅	284.2635	283.0554	–	[M – H] [–]	3.95	268.0344, 211.0333	HQ
48	Nepesaikosaponin K	C ₄₈ H ₈₀ O ₁₈	944.5345	989.5345	1.9	[M + HCOO] [–]	4.06	943.5290, 829.4599, 783.4519, 725.4124, 199.8049	CH
49	Officinalisinin I	C ₄₅ H ₇₆ O ₁₉	920.4981	959.4648	3.7	[M+K] ⁺	4.09	741.8390, 417.1752, 273.2432	ZM
50	Isoflavanone	C ₁₅ H ₁₂ O ₂	224.0837	269.0817	–0.7	[M + HCOO] [–]	4.16	193.0141, 108.0236	HQ
51	6-Methylcoumarin	C ₁₀ H ₈ O ₂	160.05243	161.0602	–0.19	[M+H] ⁺	4.21	133.0875, 105.0690	HQ
52	Anemarrhenasaponin-Ia	C ₄₀ H ₆₈ O ₁₄	772.4609	831.4751	0.4	[M + CH ₃ COO] [–]	4.49	839.4802, 785.4686, 767.4565	ZM

(continued on next page)

Table 2 (continued)

No.	Component name	Formula	Neutral mass (Da)	Observed m/z	Mass error (ppm)	Adducts	Observed RT (min)	Fragments (m/z)	Source
53	Saikosaponin F	C ₄₈ H ₈₀ O ₁₇	928.5396	973.5380	0.2	[M + HCOO] ⁻	4.68	927.5326, 781.4735, 619.4216	CH
54	Oroxylin A-7-O-glucuronide	C ₂₂ H ₂₀ O ₁₁	460.1006	483.0868	-6.3	[M+Na] ⁺	4.69	423.3765, 405.3687	HQ
55	Kaempferol ⁸	C ₁₅ H ₁₀ O ₆	286.2363	285.0276	-	[M - H] ⁻	4.7	-	CH, ZM, CH
56	Isorhamnetin ⁸	C ₁₆ H ₁₂ O ₇	316.2623	315.0424	-	[M - H] ⁻	4.84	300.0175, 285.0276	HQ, CH
57	Apigenin	C ₁₅ H ₁₀ O ₅	270.0528	315.0510	-0.2	[M + HCOO] ⁻	4.85	251.8408, 241.0652, 225.1435, 151.0348	HQ
58	Astragaloside III	C ₄₁ H ₆₈ O ₁₄	784.4609	829.4586	-0.6	[M + HCOO] ⁻	5.05	829.4602, 783.4532, 743.4594, 489.3580, 393.1592	HQ
59	Timosaponin I	C ₃₉ H ₆₆ O ₁₄	758.4453	803.4425	-1.1	[M + HCOO] ⁻	5.13	757.4374, 665.3908, 595.3806, 529.3520	ZM
60	Cubebin	C ₂₀ H ₂₀ O ₆	356.1260	355.1181	-1.7	[M - H] ⁻	5.16	161.0453	CH
61	Isoliquiritigenin	C ₁₅ H ₁₂ O ₄	256.0736	255.0663	0.1	[M - H] ⁻	5.26	213.1294	ZM
62	Anemarrhenasaponin A ₂	C ₃₉ H ₆₄ O ₁₄	756.4296	801.4273	-0.7	[M + HCOO] ⁻	5.35	635.3797, 593.3678, 375.1848	ZM
63	Sainfuran	C ₁₆ H ₁₄ O ₅	286.0841	285.0762	-2.4	[M - H] ⁻	5.43	-	CH
64	Pratensein	C ₁₆ H ₁₂ O ₆	300.0634	299.0554	-2.4	[M - H] ⁻	5.5	223.0397, 196.0490	HQ
65	Formononetin	C ₁₆ H ₁₂ O ₄	268.0736	267.0662	-0.4	[M - H] ⁻	5.54	252.0425, 223.0397, 195.0450, 167.0501	HQ
66	(-)-Catechin hydrate	C ₁₅ H ₁₄ O ₆	290.0790	291.0890	9.1	[M+H] ⁺	5.55	269.1081, 197.0906, 152.0943	CH
67	Astragaloside II	C ₄₃ H ₇₀ O ₁₅	826.4715	871.4731	3.9	[M + HCOO] ⁻	5.71	778.2931, 635.3801, 577.3384, 499.3055	HQ
68	Saikosaponin A ⁸	C ₄₂ H ₆₈ O ₁₃	780.9815	825.4397	-	[M + HCOO] ⁻	5.79	779.4495	CH
69	Saikosaponin B ₁	C ₄₂ H ₆₈ O ₁₃	780.4660	825.4650	1	[M + HCOO] ⁻	5.81	779.4588, 755.4225, 617.4057	CH
70	Saikosaponin B ₄	C ₄₃ H ₇₂ O ₁₄	812.4922	811.4896	5.8	[M - H] ⁻	5.95	753.4062, 591.3549, 267.0649, 243.8989	CH
71	Cimicifugoside	C ₃₇ H ₅₄ O ₁₁	674.3666	719.3640	-1.1	[M + HCOO] ⁻	6.1	655.3469, 520.3057, 295.2272	SM
72	Agroastragaloside I	C ₄₅ H ₇₄ O ₁₆	870.4977	915.4981	2.4	[M + HCOO] ⁻	6.2	915.4952, 419.9543, 329.2333	HQ
73	Malonylsaikosaponin A	C ₄₅ H ₇₀ O ₁₆	866.4664	865.4593	0.2	[M - H] ⁻	6.24	631.3494, 299.0907, 193.0508	CH
74	Platycoside K	C ₄₂ H ₆₈ O ₁₇	844.4457	867.4323	-3	[M+Na] ⁺	6.25	787.4346, 478.3487	JG
75	Anemarrhenasaponin III	C ₃₉ H ₆₄ O ₁₄	756.4296	801.4280	0.2	[M + HCOO] ⁻	6.37	755.4227, 635.3798, 577.3380	ZM
76	Cis-hinokiresinol	C ₁₇ H ₁₆ O ₂	252.1150	251.1077	-0.2	[M - H] ⁻	6.72	235.0763, 162.8401, 117.0348	ZM

(continued on next page)

Table 2 (continued)

No.	Component name	Formula	Neutral mass (Da)	Observed m/z	Mass error (ppm)	Adducts	Observed RT (min)	Fragments (m/z)	Source
77	Hippeastrine	C ₁₇ H ₁₇ NO ₅	315.1107	314.1019	-4.7	[M - H] ⁻	6.73	295.2269, 251.1077, 235.0763	ZM
78	Saikosaponin E	C ₄₂ H ₆₈ O ₁₂	764.4711	809.4690	-0.4	[M + HCOO] ⁻	6.75	763.4639, 753.4090, 637.3955, 619.3831	CH
79	Anemarsaponin F	C ₅₀ H ₈₂ O ₂₃	1050.5247	1095.5236	0.6	[M + HCOO] ⁻	6.83	1049.5169, 915.4600, 773.4369, 721.3797, 617.3706	ZM
80	6''-O-Acetylsaikosaponin b3	C ₄₅ H ₇₄ O ₁₅	854.5028	913.5159	-0.8	[M + CH ₃ COO] ⁻	7.02	885.4846, 677.3909, 617.3681, 559.3280	CH
81	7-O-methylisomucronulatol	C ₁₈ H ₂₀ O ₅	316.1311	315.1227	-3.6	[M - H] ⁻	7.03	283.0609	HQ
82	Astragaloside IV ^a	C ₄₁ H ₆₈ O ₁₄	784.9702	783.3947	-	[M - H] ⁻	7.35	739.4159, 677.3754, 449.2163	HQ
83	25-O-Acetyl cimigenol xyloside	C ₃₇ H ₅₈ O ₁₀	662.4030	661.3932	-3.8	[M - H] ⁻	7.41	659.3799, 513.2282, 389.1742	SM
84	Saikosaponin D ^b	C ₄₂ H ₆₈ O ₁₃	780.9815	825.4397	-	[M + HCOO] ⁻	7.49	779.4495	CH
85	Timosaponin AIII ^b	C ₃₉ H ₆₄ O ₁₃	740.4347	785.4329	0	[M + HCOO] ⁻	7.87	739.4159	ZM
86	Ethyl caffeate	C ₁₁ H ₁₂ O ₄	208.0736	226.1073	-0.5	[M + NH ₄] ⁺	7.96	207.1474, 197.1642	CH
87	Diosgenin	C ₂₇ H ₄₂ O ₃	414.3134	415.3168	-9.3	[M+H] ⁺	7.97	415.3153, 378.2821, 361.2735	ZM
88	Stigmasterol	C ₂₉ H ₄₈ O	412.3705	451.3329	-1.8	[M+K] ⁺	8.24	397.2922, 335.2605, 259.2340, 97.0604	ZM, CH, SM
89	6''-O-Acetylsaikosaponin D	C ₄₄ H ₇₀ O ₁₄	822.4766	867.4751	0.4	[M + HCOO] ⁻	8.27	821.4694, 779.4586, 761.4480, 617.4050	CH
90	(+)-Anomalin	C ₂₄ H ₂₆ O ₇	426.1679	427.1780	6.6	[M+H] ⁺	8.45	317.2493, 171.1482	CH
91	27-Dexyactein	C ₃₇ H ₅₆ O ₁₀	660.3874	659.3796	-0.7	[M - H] ⁻	8.51	659.3798, 559.3257, 523.3100, 485.3272	SM
92	Cimigenol 3-O-β-D-Xylopyranoside	C ₃₅ H ₅₆ O ₉	620.3924	665.3903	-0.6	[M + HCOO] ⁻	8.75	619.3835, 595.2781, 315.2512	SM
93	Platycoside M ₁	C ₃₆ H ₅₄ O ₁₂	678.3615	696.3953	-0.1	[M + NH ₄] ⁺	8.99	263.2641, 245.2559	JG
94	Phenprobamate	C ₁₀ H ₁₃ NO ₂	179.0946	197.1271	-7	[M + NH ₄] ⁺	9.05	149.0562	HQ
95	Acetytraagaloside	C ₄₇ H ₇₄ O ₁₇	910.4926	955.4914	0.7	[M + HCOO] ⁻	9.63	909.4861, 821.4706, 603.3378, 279.2325	HQ
96	Coronaric acid	C ₁₈ H ₃₂ O ₃	296.2351	295.2279	0.2	[M - H] ⁻	10.23	277.2175, 195.1389, 116.9286	JG
97	β-Sitosterol	C ₂₉ H ₅₀ O	414.3862	453.3479	-3.1	[M+K] ⁺	10.82	277.2434, 149.0556	SM
98	7,8-Didehydrocimigenol	C ₃₀ H ₄₆ O ₅	486.3345	545.3481	-0.4	[M + CH ₃ COO] ⁻	10.96	485.3272, 445.2909, 393.1357, 185.1178	SM

(continued on next page)

Table 2 (continued)

No.	Component name	Formula	Neutral mass (Da)	Observed m/z	Mass error (ppm)	Adducts	Observed RT (min)	Fragments (m/z)	Source
99	Cimigenol	C ₃₀ H ₄₈ O ₅	488.3502	547.3637	-0.5	[M + CH ₃ COO] ⁻	11.26	487.3410, 383.2895, 279.2326, 243.8991	SM
100	Pentadecanoic acid	C ₁₅ H ₃₀ O ₂	242.2246	287.2247	6.5	[M + HCOO] ⁻	11.32	-	SM
101	Scoparone	C ₁₁ H ₁₀ O ₄	206.0579	265.0732	5.3	[M + CH ₃ COO] ⁻	12.55	265.0752	CH
102	Anhydrocaritin	C ₂₁ H ₂₀ O ₆	368.1260	427.1440	9.8	[M + CH ₃ COO] ⁻	13.47	277.2170, 251.1648, 116.9281	ZM
103	Prosaikogenin A	C ₃₆ H ₅₈ O ₈	618.4132	641.4019	-0.7	[M+Na] ⁺	13.68	457.2680, 177.1953, 93.1013	CH
104	Linolenic acid	C ₁₈ H ₃₀ O ₂	278.2246	323.2230	0.6	[M + HCOO] ⁻	14.17	323.2208, 305.2109	HQ
105	Linoleic acid	C ₁₈ H ₃₂ O ₂	280.2402	279.2329	0	[M - H] ⁻	14.62	279.2329, 211.1338, 116.9280	HQ
106	Bifendate	C ₂₀ H ₁₈ O ₁₀	418.0900	419.0984	2.6	[M+H] ⁺	14.63	338.3643, 270.3067, 245.2555, 225.0726	HQ
107	Palmitic acid	C ₁₆ H ₃₂ O ₂	256.2402	255.2326	-1.5	[M - H] ⁻	15.56	261.1982, 205.1383, 165.0720, 149.0771, 125.0043	HQ
108	Linoleyl acetate	C ₂₀ H ₃₆ O ₂	308.2715	307.2642	0	[M - H] ⁻	16.16	281.2481, 234.8201, 116.9279	CH
109	Anemarsaponin E	C ₄₆ H ₇₈ O ₁₉	934.5137	973.4805	3.7	[M+K] ⁺	16.29	905.4240, 849.4228, 734.4902	ZM
110	Chrysanthemaxanthin	C ₄₀ H ₅₆ O ₃	584.4230	607.4104	-2.9	[M+Na] ⁺	17.14	485.3876, 312.3499, 256.2919	ZM
111	Baohuoside I	C ₂₇ H ₃₀ O ₁₀	514.1839	532.2143	-6.4	[M + NH ₄] ⁺	17.8	413.2813, 149.0554	ZM
112	Hederagenin	C ₃₀ H ₄₈ O ₄	472.3553	531.3695	0.8	[M + CH ₃ COO] ⁻	18.02	416.7036, 316.7786, 216.8533	HQ
113	Mairin	C ₃₀ H ₄₈ O ₃	456.3604	455.3531	0.1	[M - H] ⁻	18.22	455.3526, 400.7358, 339.7611, 222.8403, 184.9164	HQ

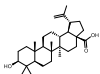
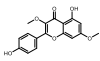
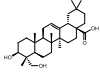
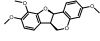
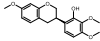
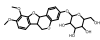
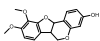
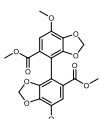
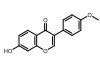
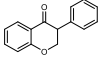
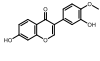
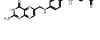
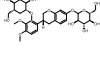
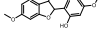
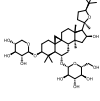
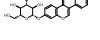
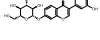
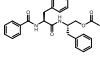
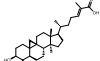
^a Compounds identified by reference compounds.

huge amounts, including astragaloside IV (M15), ononin (M16), calycosin 7-O-glucoside (M17), timosaponin B II (M28), saikosaponin A (M38), saikosaponin D (M39), rutin (M40), caffeic acid (M46), isoferulic acid (M47), ferulic acid (M48) and platycodin D (M53). Specifically, astragaloside IV, calycosin 7-O-glucoside, saikosaponin A, saikosaponin D, timosaponin B II, isoferulic acid and platycodin D have been chosen as the marker compounds for quality control of corresponding herbs in Chinese Pharmacopoeia [25]. Similarly, although ononin holds low OB value, it also exhibits remarkable pharmacological effects by alleviating H₂O₂-induced cardiomyocyte apoptosis and improving cardiac function [26]. In addition, cardioprotective effects of caffeic acid and ferulic acid are also good [27,28]. Based on the above considerations, it was reasonable to believe that 57 compounds could be listed as potentially effective compounds for SXD. Subsequently, the effective compounds of SXD were entered into the database to obtain the corresponding targets. A total of 502 SXD-related targets were screened by correcting and deleting duplicate values, which were included in the subsequent analysis.

3.3. Screening of potential targets for SXD treatment of CHD and construction of PPI network

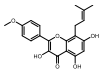
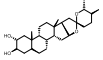
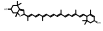
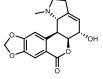
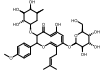
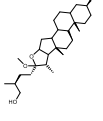
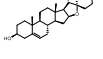
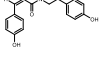
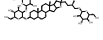
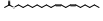
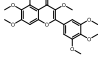
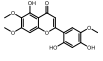
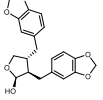
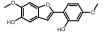
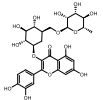
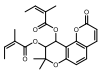
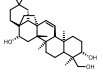
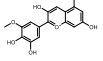
The GeneCards, OMIM, TTD and DisGeNET databases were used to search for CHD-related targets, and 610 corresponding targets were screened and sorted out. Subsequently, the 96 potential targets of SXD for the treatment of CHD were screened by getting their

Table 3
The effective compounds of SXD.

No.	Name	PubChem CID	2D structure	OB (%)	DL	Herb
M1	Mairin ^a	64971		55.38	0.78	HQ
M2	Jaranol ^a	5318869		50.83	0.29	HQ
M3	Hederagenin ^a	73299		36.91	0.75	HQ
M4	3,9-di-O-methylnissolin	15689655		53.74	0.48	HQ
M5	7-O-methylisomucronulatol ^a	15689652		74.69	0.30	HQ
M6	Methylnissolin-3-O-glucoside ^a	74977390		36.74	0.92	HQ
M7	Methylnissolin ^a	5319733		64.26	0.42	HQ
M8	Bifendate ^a	108213		31.10	0.67	HQ
M9	Formononetin ^a	5280378		69.67	0.21	HQ
M10	Isoflavanone ^a	160767		109.99	0.30	HQ
M11	Calycosin ^a	5280448		47.75	0.24	HQ
M12	Folic acid	135398658		68.96	0.71	HQ
M13	Isomucronulatol-7,2'-di-O-glucosiole	15689653		49.28	0.62	HQ
M14	1,7-Dihydroxy-3,9-dimethoxy pterocarpene	5316760		39.05	0.48	HQ
M15	Astragaloside IV ^a	13943297		22.50	0.15	HQ
M16	Ononin ^a	442813		11.52	0.78	HQ
M17	Calycosin 7-O-glucoside ^a	5318267		5.49	0.81	HQ
M18	Asperglaucide ^a	10026486		58.02	0.52	ZM
M19	Mangiferolic acid	45270099		36.16	0.84	ZM

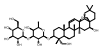
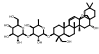
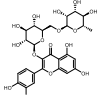
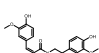
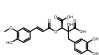
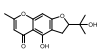
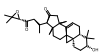
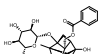
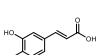
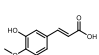
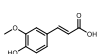
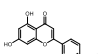
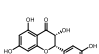
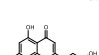
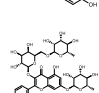
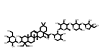
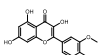
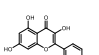
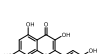

(continued on next page)

Table 3 (continued)

No.	Name	PubChem CID	2D structure	OB (%)	DL	Herb
M20	Anhydroicaritin ^a	5318980		45.41	0.44	ZM
M21	Anemarsaponin F _{qt} ^a	/		60.06	0.79	ZM
M22	Chrysanthemaxanthin ^a	21160900		38.72	0.58	ZM
M23	Hippeastrine ^a	441594		51.65	0.62	ZM
M24	Icariin I ^a	/		41.58	0.61	ZM
M25	Anemarsaponin E _{qt} ^a	/		30.67	0.86	ZM
M26	Diosgenin ^a	99474		80.88	0.81	ZM
M27	Coumaroyltyramine ^a	/		112.9	0.20	ZM
M28	Timosaponin B II ^a	44575945		13.87	0.04	ZM
M29	Linoleyl acetate ^a	21159087		42.10	0.20	CH
M30	3',4',5',3,5,6,7-Heptamethoxyflavone ^a	389001		31.97	0.59	CH
M31	Areapillin	158311		48.96	0.41	CH
M32	Cubebin ^a	117443		57.13	0.64	CH
M33	Sainfuran ^a	185034		79.91	0.23	CH
M34	Troxeutin	252216528		31.6	0.28	CH
M35	(+)-Anomalin ^a	6450453		46.06	0.66	CH
M36	Saikosaponin C _{qt}	/		30.50	0.63	CH
M37	Petunidin	441774		30.05	0.31	CH

(continued on next page)

Table 3 (continued)

No.	Name	PubChem CID	2D structure	OB (%)	DL	Herb
M38	Saikosaponin A ^a	167928		32.39	0.09	CH
M39	Saikosaponin D ^a	107793		34.39	0.09	CH
M40	Rutin ^a	5280805		3.20	0.68	CH
M41	Tuberosine A ^a	5322166		102.67	0.34	SM
M42	Cimicifugic acid	100913813		83.02	0.45	SM
M43	Visamminol	5315249		50.01	0.23	SM
M44	(20r,24r)-24,25-epoxy-3-beta-(beta-d-xylopyranosyloxy)-9,19-cyclolanost-7-ene-16,23-dione Qt	/		40.10	0.76	SM
M45	Paeoniflorin ^a	442534		53.87	0.79	SM
M46	Caffeic acid ^a	689043		25.76	0.05	SM
M47	Isoferulic acid ^a	736186		58.83	0.06	SM
M48	Ferulic acid ^a	445858		54.79	0.06	SM
M49	Acacetin ^a	5280442		34.97	0.24	JG
M50	Cis-Dihydroquercetin	443758		66.44	0.27	JG
M51	Luteolin ^a	5280445		36.16	0.25	JG
M52	Robinin	5281693		39.84	0.71	JG
M53	Platycodin D	162859		7.60	0.01	JG
M54	Isorhamnetin ^a	5281654		49.6	0.31	HQ, CH
M55	Kaempferol ^a	5280863		41.88	0.24	HQ, ZM, CH
M56	Quercetin ^a	5280343		46.43	0.28	HQ, CH
M57	Stigmasterol ^a	5280794		43.83	0.76	ZM, CH, SM

^a Compounds identified by UPLC-Q-TOF/MS.

intersection targets (Fig. 2A). The 96 potential targets in herbs and diseases accounted for 19.12 % and 15.74 %, respectively. Among the 96 potential targets, the number of potential targets of each herb in SXD was shown in Fig. 2B. HQ, ZM, CH, SM and JG accounted for 90.62 %, 44.79 %, 82.29 %, 46.88 % and 27.08 % of the potential targets, respectively, which implied that the herbs contained potential targets with the same effect. HQ, as a monarch herb in SXD, contained more potential targets than other herbs, and had a synergistic effect with the 72 and 21 overlapping targets of CH and SM, respectively. Similarly, ZM and JG, as assistant and guide herbs in the prescription, could also assist the monarch herb to exert a therapeutic effect. This was also in line with the characteristics of TCM prescriptions for the synergistic treatment of diseases.

The 96 potential targets were imported into the STRING database, and the medium confidence (0.4) between the targets was set to obtain a PPI network file, which was imported into Cytoscape 3.8.2 software for visualization. The PPI network involves 96 nodes and 1671 edges, and the average degree and betweenness centrality of all nodes are 34.8125 and 0.0132, respectively (Fig. 2C). In order to further understand the biological role of the PPI network, the constructed PPI network was used as input to conduct network clustering analysis based on MCODE cluster, and a total of 3 network clusters were identified. According to the MCODE score, the largest cluster contained 46 nodes and 885 edges, with a score of 39.333, and the smallest cluster contained 8 nodes and 13 edges, with a score of 3.714. The targets in the PPI network are greater than the average of degree and betweenness centrality and included in the core sub-networks cluster as key targets, which are TNF, IL-6, peroxisome proliferator-activated receptor alpha (PPARG), TP53, RAC-alpha serine/threonine-protein kinase (AKT1), angiotensin-converting enzyme 2 (ACE), IL-1β, nitric oxide synthase, endothelial (NOS3), estrogen receptor (ESR1), epidermal growth factor receptor (EGFR), vascular endothelial growth factor A (VEGFA), prostaglandin G/H synthase 2 (PTGS2) and catenin beta-1 (CTNNB1). The key targets possess a higher degree value and are more likely to play a critical role in the network of SXD acting on CHD. Meanwhile, the S-value of each key target was the maximum value of 4 by CytoHubba plugin analysis excluding ESR1, EGFR and CTNNB1, and then the S-value of each target in the PPI network was analyzed (Table 4).

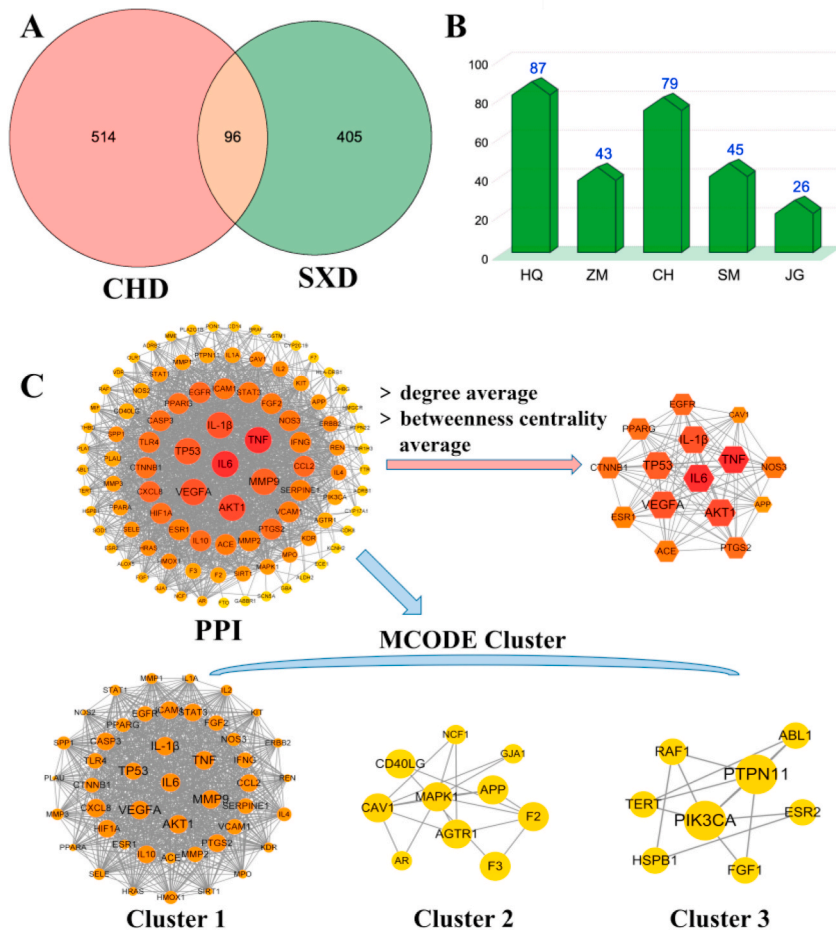


Fig. 2. Analysis of potential targets for SXD against CHD. (A) Venn diagram of SXD and CHD related targets; (B) Distribution of potential targets of each herb in SXD; (C) PPI network analysis of potential targets for SXD against CHD (The red hexagon nodes represent the 15 key targets with the average of degree and betweenness in the topology analysis. MCODE was used to reclassify existing potential targets).

Table 4
Potential targets of SXD against CHD and their weight analysis.

No.	Target	UniProt ID	Gene name	Degree	S-value
T1	RAC-alpha serine/threonine-protein kinase	P31749	AKT1	73	4
T2	Tumor necrosis factor	P01375	TNF	80	4
T3	Interleukin-8	P10145	IL-8	63	4
T4	Interleukin-6	P05231	IL-6	80	4
T5	Interleukin-1 beta	P01584	IL-1 β	70	4
T6	Vascular endothelial growth factor A	P15692	VEGFA	70	4
T7	Cellular tumor antigen p53	P04637	TP53	67	4
T8	Matrix metalloproteinase-9	P14780	MMP9	64	3
T9	C-C motif chemokine 2	P13500	CCL2	62	4
T10	Signal transducer and activator of transcription 3	P40763	STAT3	56	3
T11	Epidermal growth factor receptor	P00533	EGFR	62	3
T12	Vascular cell adhesion protein 1	P19320	VCAM1	54	3
T13	Caspase-3	P42574	CASP3	59	4
T14	Toll-like receptor 4	O00206	TLR4	58	4
T15	Interleukin-10	P22301	IL10	60	3
T16	Fibroblast growth factor 2	P09038	FGF2	55	4
T17	Prostaglandin G/H synthase 2	P35354	PTGS2	60	4
T18	Catenin beta-1	P35222	CTNNB1	58	3
T19	Nitric oxide synthase, endothelial	P29474	NOS3	56	4
T20	Intercellular adhesion molecule 1	P05362	ICAM1	57	4
T21	Peroxisome proliferator-activated receptor gamma	P37231	PPARG	59	4
T22	Hypoxia-inducible factor 1-alpha	Q16665	HIF1A	59	4
T23	72 kDa type IV collagenase	P08253	MMP2	51	3
T24	Plasminogen activator inhibitor 1	P05121	SERPINE1	52	4
T25	Interleukin-4	P05112	IL-4	49	3
T26	Interferon gamma	P01579	IFNG	53	4
T27	Interleukin-2	P60568	IL-2	45	4
T28	E-selectin	P16581	SELE	43	3
T29	GTPase HRas	P01112	HRAS	45	3
T30	Estrogen receptor	P03372	ESR1	51	3
T31	Osteopontin	P10451	SPP1	45	4
T32	Angiotensin-converting enzyme 2	Q9BYF1	ACE	54	4
T33	Heme oxygenase 1	P09601	HMOX1	46	4
T34	Caveolin-1	Q03135	CAV1	46	3
T35	Vascular endothelial growth factor receptor 2	P35968	KDR	42	4
T36	Receptor tyrosine-protein kinase erbB-2	P04626	ERBB2	47	3
T37	Renin	P00797	REN	43	4
T38	Myeloperoxidase	P05164	MPO	43	3
T39	Interleukin-1 alpha	P01583	IL1A	37	4
T40	Peroxisome proliferator-activated receptor alpha	Q07869	PPARA	39	3
T41	Mast/stem cell growth factor receptor Kit	P10721	KIT	40	3
T42	Stromelysin-1	P08254	MMP3	38	4
T43	Signal transducer and activator of transcription 1-alpha/beta	P42224	STAT1	41	3
T44	Interstitial collagenase	P03956	MMP1	36	4
T45	NAD-dependent protein deacetylase sirtuin-1	Q96E86	SIRT1	41	4
T46	Tissue factor	P13726	F3	33	1
T47	Nitric oxide synthase, inducible	P35228	NOS2	31	1
T48	Urokinase-type plasminogen activator	P00749	PLAU	32	1
T49	Mitogen-activated protein kinase 1	P28482	MAPK1	40	2
T50	Prothrombin	P00734	F2	34	2
T51	Tyrosine-protein phosphatase non-receptor type 11	Q06124	PTPN11	33	0
T52	Amyloid-beta precursor protein	P05067	APP	40	3
T53	Type-1 angiotensin II receptor	P30556	AGTR1	30	0
T54	CD40 ligand	P29965	CD40LG	29	0
T55	Neutrophil cytosol factor 1	P14598	NCF1	27	1
T56	Phosphatidylinositol 4,5-bisphosphate 3-kinase catalytic subunit alpha isoform	P42336	PIK3CA	33	0
T57	Heat shock protein beta-1	P04792	HSPB1	24	1
T58	Gap junction alpha-1 protein	P17302	GJA1	27	1
T59	Androgen receptor	P10275	AR	28	1
T60	Estrogen receptor beta	Q92731	ESR2	24	0
T61	Telomerase reverse transcriptase	O14746	TERT	24	0
T62	Tissue-type plasminogen activator	P00750	PLAT	24	0
T63	Superoxide dismutase [Cu-Zn]	P00441	SOD1	24	1
T64	Macrophage migration inhibitory factor	P14174	MIF	23	1
T65	Polyunsaturated fatty acid 5-lipoxygenase	P09917	ALOX5	24	0
T66	Thrombomodulin	P07204	THBD	23	1
T67	Fibroblast growth factor 1	P05230	FGF1	24	0
T68	Vitamin D3 receptor	P11473	VDR	20	1

(continued on next page)

Table 4 (continued)

No.	Target	UniProt ID	Gene name	Degree	S-value
T69	Tyrosine-protein kinase ABL1	P00519	ABL1	24	0
T70	RAF proto-oncogene serine/threonine-protein kinase	P04049	RAF1	22	0
T71	Oxidized low-density lipoprotein receptor 1	P78380	OLR1	19	1
T72	Phospholipase A2	P04054	PLA2G1B	17	1
T73	Neprilysin	P08473	MME	17	0
T74	Beta-2 adrenergic receptor	P07550	ADRB2	18	0
T75	Monocyte differentiation antigen CD14	P08571	CD14	14	0
T76	Serum paraoxonase/arylesterase 1	P27169	PON1	15	1
T77	Serine/threonine-protein kinase B-raf	P15056	BRAF	12	1
T78	HLA class II histocompatibility antigen, DRB1 beta chain	P01911	HLA-DRB1	10	0
T79	Tyrosine-protein phosphatase non-receptor type 22	Q9Y2R2	PTPN22	9	0
T80	Oxysterols receptor LXR-alpha	Q13133	NR1H3	8	0
T81	Coagulation factor VII	P08709	F7	10	1
T82	3-hydroxy-3-methylglutaryl-coenzyme A reductase	P04035	HMGCR	9	1
T83	Glutathione S-transferase Mu 1	P09488	GSTM1	10	0
T84	Beta-1 adrenergic receptor	P08588	ADRB1	8	0
T85	Sex hormone-binding globulin	P04278	SHBG	10	0
T86	Cyclin-dependent kinase 8	P49336	CDK8	6	1
T87	Cytochrome P450 2C19	P33261	CYP2C19	10	1
T88	Transthyretin	P02766	TTR	8	1
T89	Steroid 17-alpha-hydroxylase/17,20 lyase	P05093	CYP17A1	7	1
T90	Lysosomal acid glucosylceramidase	P04062	GBA	3	0
T91	Potassium voltage-gated channel subfamily H member 2	Q12809	KCNH2	4	1
T92	Endothelin-converting enzyme 1	P42892	ECE1	3	0
T93	Sodium channel protein type 5 subunit alpha	Q14524	SCN5A	3	1
T94	Gamma-aminobutyric acid type B receptor subunit 1	Q9UBS5	GABBR1	2	0
T95	Aldehyde dehydrogenase, mitochondrial	P05091	ALDH2	3	0
T96	Alpha-ketoglutarate-dependent dioxygenase FTO	Q9C0B1	FTO	1	0

3.4. C-T-D network construction and CI analysis

A C-T-D network was constructed by the Cytoscape 3.8.2 software to facilitate the visualization and interpretation of the complex relationships according to the corresponding information, including effective compounds, potential targets and related diseases of SXD, which consisted of 159 nodes (96 target nodes, 57 compound nodes, 5 herb nodes and 1 disease node) and 523 edges (Fig. 3A). Most targets were shared by candidate effective compounds of each herb in SXD. The high interconnectedness of the C-T-P network was due to the high interconnection degrees of these candidate effective compounds, including quercetin (M56, degree = 51), luteolin (M51, degree = 23), ferulic acid (M48, degree = 19), isoferulic acid (M47, degree = 19), caffeic acid (M46, degree = 17), kaempferol (M55, degree = 13) and anhydrocaritin (M20, degree = 13). Subsequently, we calculated the parameters of the C-T-D network by using NetworkAnalyzer function and analyze the RSR of parameters by the SPSS AU platform (Table S1). Quercetin, the compound

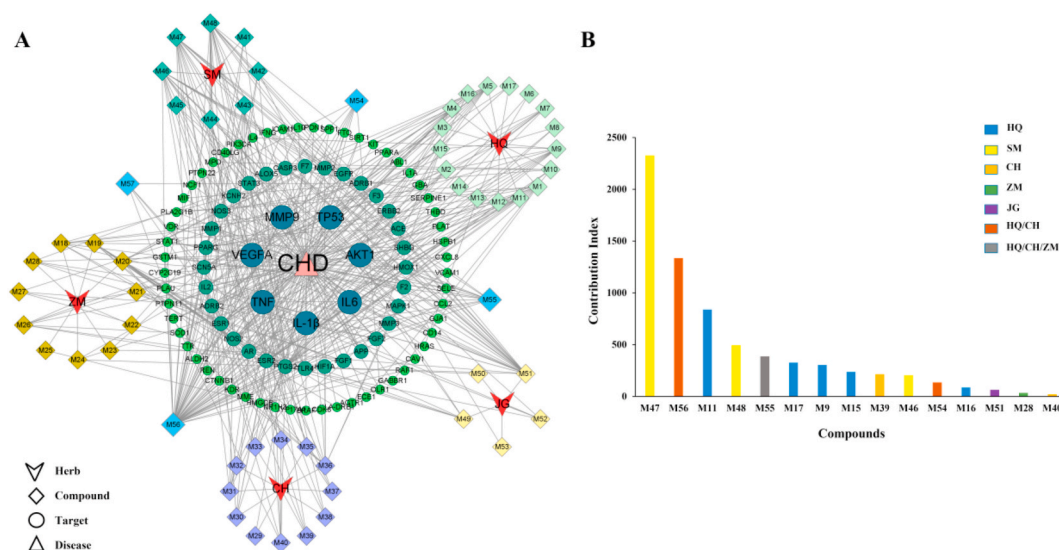


Fig. 3. Screening of core compounds for SXD against CHD. (A) C-T-D network for SXD against CHD (The blue diamond represents a compound shared by two or more herbs); (B) Contribution index of each effective compound (top 15) for SXD against CHD.

with the largest degree in the C-T-D network, only ranked 12 according to RSR. However, the compound anhydroicaritin, the seventh-ranked degree in the network, ranked the highest RSR value. So, a more systematic and accurate index was needed to screen effective compounds in SXD. Based on the network parameters, the content and pharmacokinetic parameter of the compounds in SXD, CI was proposed to screen the core compounds (Tables S2 and S3). Isoferulic acid (M47), quercetin (M56), calycosin (M11), ferulic acid (M48), kaempferol (M55), calycosin 7-O-glucoside (M17), formononetin (M9), astragaloside IV (M15) and saikosaponin D (M39), were ranked as the top 9 compounds according to the accumulative CI value more than 90 %, which could be the core compounds of SXD in the treatment of CHD (Fig. 3B). In addition, among the top 15 effective compounds in the CI value ranking, the emperor herb HQ contained 7 effective compounds, and CH and SM as the minister herbs contained 4 and 3 effective compounds, respectively.

3.5. Enrichment analyses and construction of T-P network

The 96 potential targets were entered into the DAVID database for GO and KEGG enrichment analysis. The GO enrichment analysis results were reflected in three aspects: BP, CC and MF. Under the condition of $p < 0.05$, 640, 63 and 101 items were obtained from these three aspects, respectively. The top 10 items were taken to make a visual bar chart using the bioinformatics platform, as shown in Fig. 4A, which indicated that SXD may regulate ERK1 and ERK2 cascade, transcription from RNA polymerase II promoter, MAPK cascade, RNA polymerase II transcription factor activity, protein binding, and perinuclear region of cytoplasm for treating CHD. Moreover, a total of 155 pathways were identified by KEGG analysis. All the pathways involved in the S-value of potential targets were ranked and analyzed. Based on the $p < 0.05$, the top 20 pathways enriched by KEGG were selected according to the P-weight, as shown in Fig. 4B and C and Table S4. Among them, fluid shear stress and atherosclerosis, lipid and atherosclerosis, PI3K-Akt signaling pathway, MAPK signaling pathway, HIF-1 signaling pathway, and EGFR tyrosine kinase inhibitor resistance were probably associated with SXD against CHD.

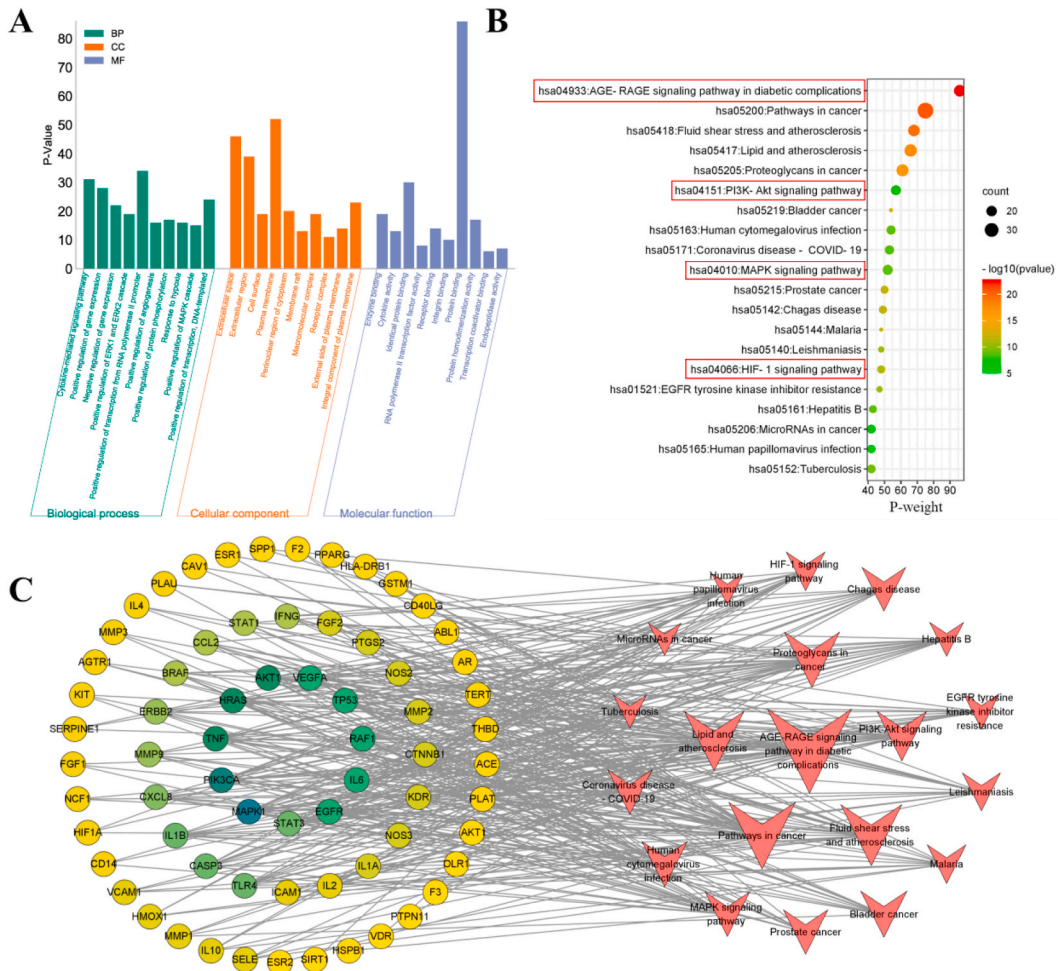


Fig. 4. Potential targets enrichment analysis and T-P network analysis of SXD treatment for CHD. (A, B) GO and KEGG enrichment analysis for SXD against CHD; (C) T-P network of SXD against CHD where the size of pathway node is based on the P-weight, and the color of the target node represents the degree value.

3.6. Core targets expression analysis

In GSE66360, we analyzed the expression of key targets in MI samples ($n = 49$) and control samples ($n = 50$). As shown in Fig. 5, the expression levels of TNF, IL-6, IL-1 β , PTGS2 and VEGFA were up-regulated than those of the control group ($p < 0.05$), while the expression level of TP53 was down-regulated ($p < 0.05$). There was no significant difference in the expression levels of other key targets ($p > 0.05$). Therefore, we considered the targets with significant expression differences as core targets. Subsequently, the core targets were entered into the VaeElect database to obtain the correlation score between the core targets and the disease (Table S5). Obviously, we found that the average disease's causing likelihood of IL-1 β was as high as 81.8 %, but that of IL-6 was relatively low, which was only 56.1 %. Therefore, these core targets were used as the main targets of SXD against CHD and included in subsequent analysis.

3.7. Analysis of molecular docking results

Molecular docking is the docking of ligands and receptors in the active pocket through one or more hydrogen bonds, which is a process accompanied by a change in binding energy. In order to verify the reliability of the network pharmacology research results, these core targets, TNF (PDB ID: 7KP9), IL-6 (PDB ID: 4O9H), IL-1 β (PDB ID: 5I1B), VEGFA (PDB ID: 5DN2), TP53 (PDB ID: 5AOI) and PTGS2 (PDB ID: 5F19) were selected as receptors, and they were docked with the core compounds in Fig. 6A. In general, when the ligand-receptor binding energy is lower than 0, the binding energy is about the greater the possibility of interaction. When the binding energy is lower than -5.0 kcal/mol, it contains good affinity. For these effective compounds, quercetin, calycosin, kaempferol, calycosin 7-*O*-glucoside, formononetin, astragaloside IV and saikosaponin D could produce lower binding activity with most targets, especially with TNF and PTGS2. Among them, calycosin 7-*O*-glucoside have the lowest docking binding energy to PTGS2 (-11.3 kcal/mol), and isoferulic acid has the highest binding energy to IL-6 (-5.2 kcal/mol). Subsequently, six results with relatively low binding energy of core targets were selected for visualization. As shown in Fig. 6B, calycosin7-*O*-glucoside could interact with Lys11 (B), Leu157 (A) and Leu (B) via one hydrogen bonds in TNF, respectively. Astragaloside IV was more capable of interacting with Gly42 (H) via two hydrogen bonds and with Ley175 (H), Ala173 (H), Lys169 (L), Gly43 (L) and Gln39 (H) via one hydrogen bond in IL-6. Calycosin 7-*O*-glucoside could interact with Tyr90 (A), Pro87 (A), Glu64 (A), Ser5 (A), Lys65 (A) and Tyr68 (A) via one or two hydrogen bonds in IL-1 β . The results of the interaction of VEGFA, TP53 and PTGS2 with the core compounds were also seen in Fig. 6B. Therefore, these results suggested a strong binding between core compound-target pairs and demonstrated that the target proteins were in a favorable conformation.

3.8. Experimental verification

3.8.1. SXD ameliorates the myocardial injury and inflammatory response in CHD model rats

As shown in Fig. 7A, HWI in the CHD model group was significantly higher than that in the sham-operated group. Compared with the CHD model group, the HWI levels of Bet and SXD groups were reduced to different degrees. TTC staining was used to evaluate myocardial infarct size. Compared with sham-operated group, myocardial infarction size was significantly increased in CHD model group, while myocardial infarction size decreased after SXD treatment (Fig. 7B). In the CHD model group, H&E and Masson staining

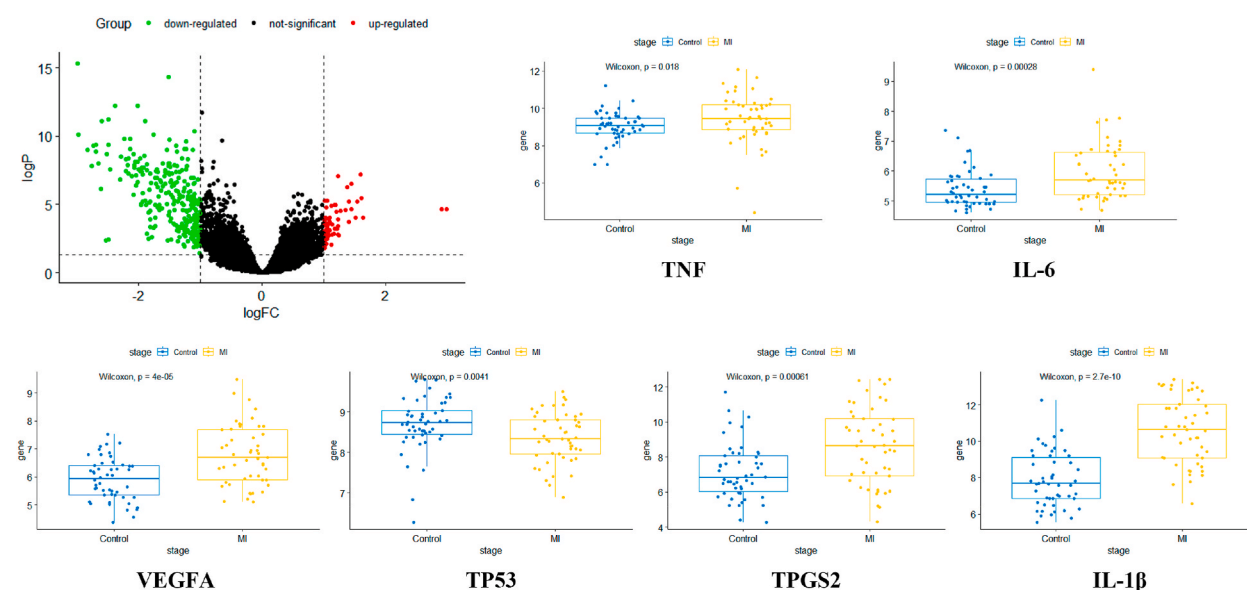


Fig. 5. Analysis of core targets expression based on GEO dataset (The values of $p < 0.05$ was considered to be significant expression differences).

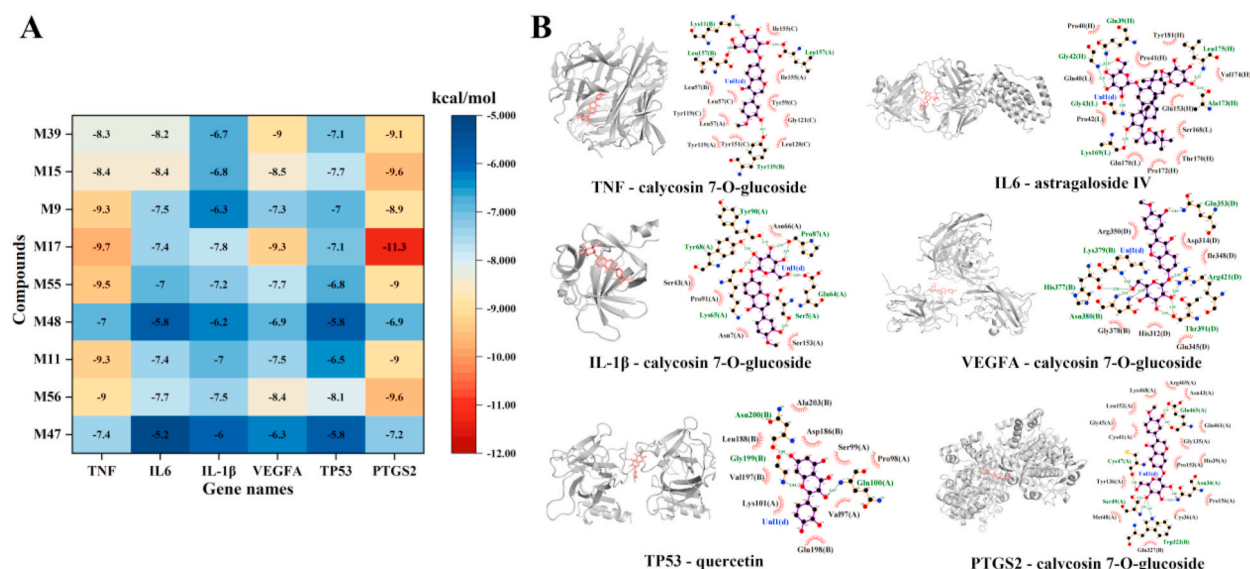


Fig. 6. Molecular docking of the core compound-target pair of SXD treatment for CHD. (A) Heat map of estimated binding energy where colour change from blue to red indicates binding energy from high to low. (B) Molecular docking of core compounds of SXD and receptor proteins.

showed severe necrosis of myocardial fibers, inflammatory cell infiltration, and tissue structure disorder. The degree of tissue fibrosis and cell damage were significantly improved in Bet and SXD groups (Fig. 7C). In addition, serum IL-1 β and IL-6 levels were increased in the CHD model group compared to the Sham group ($p < 0.01$). Compared with the model group, the levels of serum IL-1 β and IL-6 in each dosing group were decreased to varying degrees (Fig. 7D). In addition, SXD could also change the levels of serum ALD, Ang II and NT-proBNP in CHD rats. The results showed that SXD significantly reduces HWI, alleviates myocardial tissue injury and reduces the level of serum inflammation in CHD rats.

3.8.2. SXD effectively enhances cell viability and decreases the production of ROS

To identify the most effective concentration of SXD for myocardial protection, the MTT method was used. Compared with the control group, the H/R-induced cardiomyocytes showed lower cell viability (Fig. 8A). In the H/R + Diazoxide groups comparing with the H/R group, Diazoxide increased the viability. Further, a 24 h pretreatment with SXD at various concentrations (250 $\mu\text{g}/\text{mL}$, 500 $\mu\text{g}/\text{mL}$ and 1 mg/mL) significantly increased cell viability, compared with the H/R group ($p < 0.05$). Thus, the concentrations of 250 $\mu\text{g}/\text{mL}$, 500 $\mu\text{g}/\text{mL}$ and 1 mg/mL of SXD were selected to explore the possible mechanism. To confirm that SXD could protect H9c2 cells through anti-oxidative activity, we analyzed the ROS production (Fig. 8B and S2). As shown in Fig. 8B, the ROS level was higher in the H/R group than control, while SXD markedly decreased the production of ROS in H/R stimulated H9c2 cells.

3.8.3. SXD protects H9c2 cells from H/R-induced myocardial damage

Meanwhile, to investigate the anti-apoptotic effect of SXD, flow cytometry was used. As displayed in Fig. 8C, compared with the control group, the number of apoptotic cells increased in the H/R group, whereas pretreatment with SXD reduced the apoptotic ratio ($p < 0.01$). Collectively, these data show that SXD can reduce the cellular apoptosis induced by H/R.

Moreover, three different proinflammatory cytokines (TNF, IL-6 and IL-1 β) were detected, and as shown in Fig. 8D, ELISA proved that the contents of TNF, IL-6 and IL-1 β in H9c2 cells culture supernatant were reduced in SXD-treated H9c2 cells, as compared to H/R-induced H9c2 cells ($p < 0.01$). The results showed that H/R-stimulated production of TNF, IL-6 and IL-1 β in H9c2 cells were abolished by SXD.

3.8.4. The expression of mRNA and protein during the H/R-induced inhibition of apoptosis

It was found that ROS production and DNA damage activated the TP53 signaling pathway, and TP53 further up-regulated cytochrome C-mediated caspase-3 activation, leading to apoptosis [29]. TP53, caspase3 and cytochrome C mRNA expression levels were examined in order to further clarify the molecular mechanism of the H/R-induced inhibition of apoptosis. RT-qPCR results in Fig. 9A showed that TP53 expression was significantly up-regulated in the H/R group ($p < 0.01$), and this expression was dramatically reversed by SXD treatment at a concentration of 500 $\mu\text{g}/\text{mL}$ and 1 mg/mL for 24 h ($p < 0.01$). However, no obvious difference in TP53 expression was observed between the groups treated with SXD at 250 $\mu\text{g}/\text{mL}$, diazoxide and the H/R group, separately ($p > 0.05$). RT-qPCR results showed that caspase3 expression was significantly up-regulated in the H/R group ($p < 0.01$) and this expression was dramatically reversed by treatment with SXD at 250 $\mu\text{g}/\text{mL}$, 500 $\mu\text{g}/\text{mL}$ and 1 mg/mL for 24 h ($p < 0.01$). RT-qPCR results showed that cytochrome C expression was significantly up-regulated in the H/R group ($p < 0.01$) and this expression was dramatically reversed by treatment with SXD at 250 $\mu\text{g}/\text{mL}$, 500 $\mu\text{g}/\text{mL}$ and 1 mg/mL for 24 h ($p < 0.01$). However, no significant difference in caspase3 and

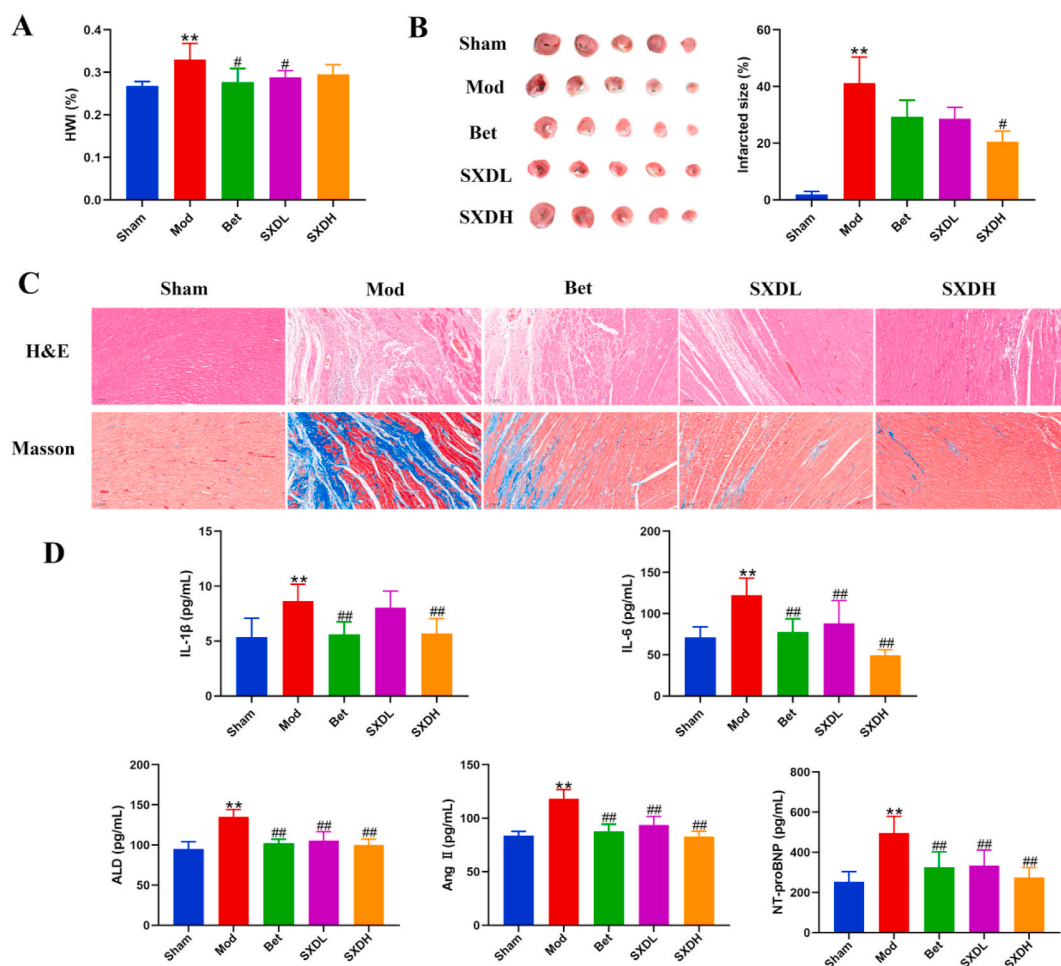


Fig. 7. SCD significantly alleviates myocardial injury and inflammatory response in CHD rats. Sham: Sham operation group; Mod: CHD model group; Bet: Betaloc group (10 mg/kg); SXDL: SCD low-dose group (4.33 g/kg); SXDH: SCD high-dose group (12.99 g/kg). (A) Heart weight index ($n = 6$); (B) Infarct size of heart tissue ($n = 3$); (C) H&E and Masson staining of the heart tissue; (D) ELISA was performed to examine the contents of IL-6, IL-1 β , ALD, Ang II and NT-proBNP in the rat serum ($n = 6$). * $p < 0.05$, ** $p < 0.01$, vs. Control; # $p < 0.05$, ## $p < 0.01$, vs. H/R.

cytochrome C expression was observed between the groups treated with diazoxide and the H/R group.

To further elucidate the mechanism by which SCD protect the H/R-induced inhibition of apoptosis, we analyzed the expression of caspase3, caspase9 and cytochrome C that regulate cellular apoptosis using western blotting analysis. The results revealed that the expression of caspase3, caspase9 and cytochrome C were significantly decreased by SCD treatment for 24 h compared with the H/R-induced H9c2 cells model group, especially when the concentration was 1 mg/mL in Fig. 9B (The uncropped versions of Fig. 9B was provide as Supplement Fig. S3). Additionally, the activity of caspase3 in H/R-induced H9c2 cells culture supernatant were reduced in SCD-treated H9c2 cells, as compared to H/R-induced H9c2 cells in Fig. 9C ($p < 0.05$). In summary, these data indicate that SCD significantly relieve myocardial injury from the perspective of anti-apoptosis via down-regulating the caspase3, caspase9 and cytochrome C protein expression levels.

4. Discussion

CHD is a complex cardiovascular disease that seriously threatens human health. The pathological mechanism of CHD is in line with the pathogenic characteristics of the “qi” stagnation. The Chinese medicine understanding of the “qi” stagnation will cause the weak and slow blood flow and abnormal hemorheology. Therefore, treating this disease from the “qi” stagnation and blood stasis has important practical significance for the diagnosis and treatment of modern CHD. Treating this disease from the “qi” stagnation and blood stasis has important practical significance for the diagnosis and treatment of modern CHD. SCD is a classic TCM prescription and possesses the effect of nourishing the “qi” and blood for the body. SCD, which is composed of *Astragalus membranaceus* var. *mongholicus* (Bunge) Hsiao (HQ), *Anemarrhena asphodeloides* Bge. (ZM), *Bupleurum chinense* DC. (CH), *Platycodon grandiflorum* (Jacq.) A. DC. (JG) and *Cimicifuga foetida* L. (SM), has been successfully applied in clinical treatment of CHD [30]. The combination of each herb in SCD

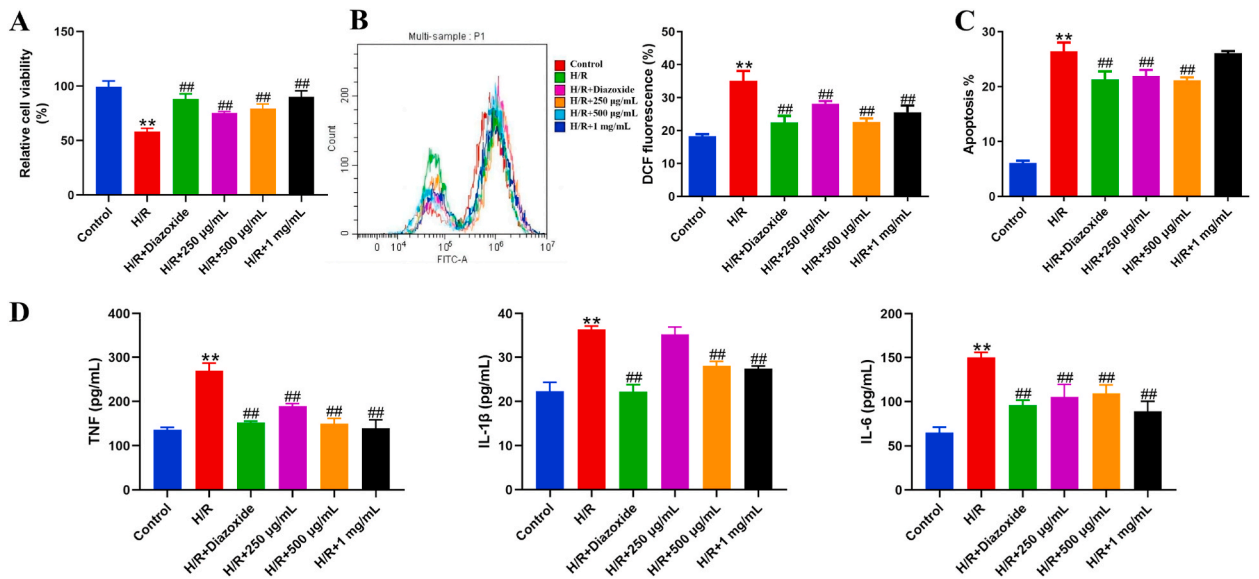


Fig. 8. SxD increases cell viability and attenuates H/R-induced H9c2 cell injury. (A) The viability of cardiomyocyte cell line H9c2 after treated with H/R or SxD was determined by MTT assays (n = 5); (B) ROS levels were detected by flow cytometry (n = 3); (C) Effects of SxD on the apoptosis ratio of H9c2 cells (n = 3); (D) ELISA was performed to examine the contents of TNF, IL-6 and IL-1 β in H9c2 cells culture supernatant (n = 3). * p < 0.05, ** p < 0.01, vs. Control; # p < 0.05, ## p < 0.01, vs. H/R.

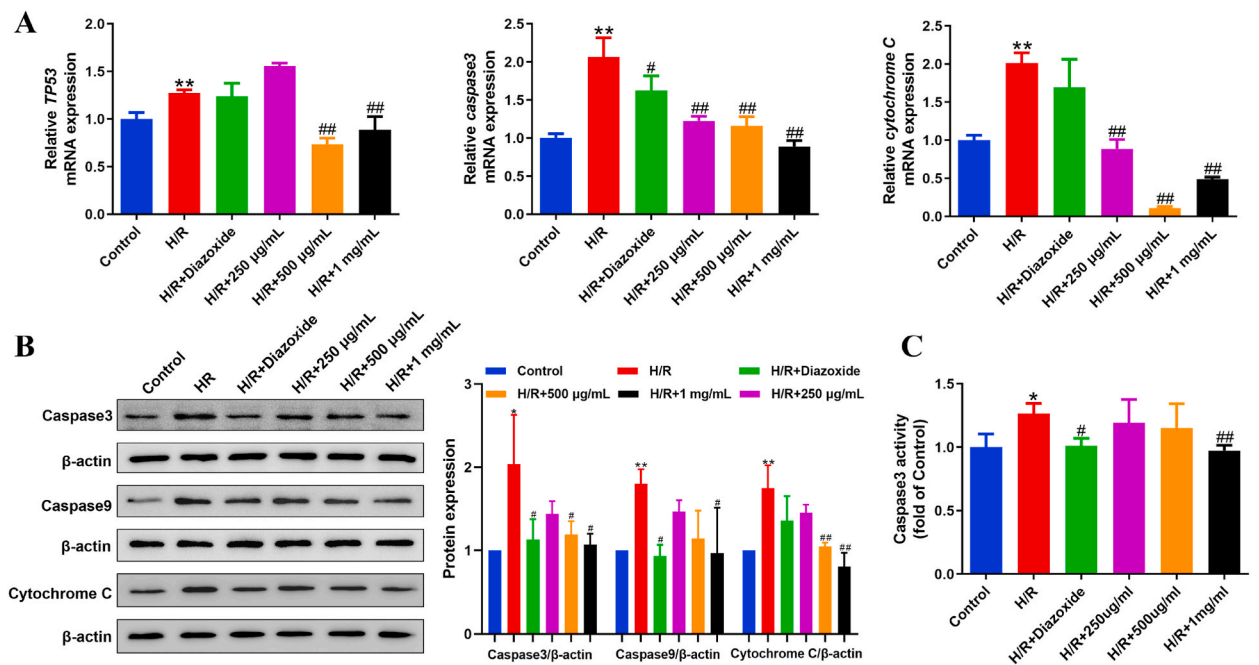


Fig. 9. The expression of mRNA and protein during the H/R-mediated inhibition of apoptosis. (A) The mRNA expressions of TP53, caspase3 and cytochrome C in H/R-induced cardiomyocyte cell line H9c2 after treated with SxD were determined (n = 3); (B) Western blotting analysis detected the caspase3, caspase9 and cytochrome C protein expression levels in H/R-induced H9c2 cells after treated with SxD (n = 3); (C) Activity Assay Kit was performed to examine the activity of caspase3 in H/R-induced cardiomyocyte cell line H9c2 after treated with SxD (n = 3). * p < 0.05, ** p < 0.01, vs. Control; # p < 0.05, ## p < 0.01, vs. H/R.

has a synergistic effect on the treatment. Research has indicated that JG can enhance the distribution or absorption of SxD, which reflects the courier role of PG [10]. SxD has not been found to be used in other countries. But it should be noted that those plants used for the preparation of SxD was not unique for TCM. They also have been used in other countries, including Japan, Korea, Russia and

other regions [31–34]. For example, HQ is included in the Japanese Pharmacopoeia, and the team from Japan investigated the different protective effects of astragalus [31,32]. In addition, CH, which is widespread in the eastern regions of Russia as well as in Mongolia and Korea, have been widely applied as a choleric and hepatoprotective remedy in traditional Russian medicine [33]. The standardized DA-9805 consists of CH from Dong-A ST (Yongin, Korea) can protect dopaminergic neurons against 6-hydroxydopamine in a Parkinson's model of neurotoxic disease [34]. At present, SXD is widely used in the treatment of CHD, but its therapeutic mechanism is not clear. The purpose of this study is to provide scientific basis for the treatment of SXD with CHD.

In this study, through the combination of UPLC-Q-TOF-MS/MS technology and an integrated network pharmacology, we directly identified the potential active ingredients and targets of SXD in the treatment of CHD from a large number of data, and understood the molecular mechanism and important pathways of TCM. 57 effective compounds and 96 corresponding potential targets were selected, which were largely involved in multiple biological processes and pathways associated with CHD. To better understand the contribution of compounds in SXD, we introduced a parameter CI that simulated compatible combinations of effective compounds in SXD in terms of intrinsic properties and network importance. From the C-T-D network and CI calculation, it was revealed that the core compounds, including isoferulic acid, quercetin, calycosin, ferulic acid, kaempferol, calycosin 7-O-glycoside, formononetin, astragaloside IV and saikosaponin D, were ranked as the top 9 compounds according to the sum of their CI value more than 90%. The core compounds were the main compounds of SXD in the treatment of CHD. Pharmacological studies have shown that the emperor herb HQ in SXD and its compounds have various biological activities, such as regulating immunity, anti-oxidation, anti-inflammatory, anti-apoptosis and preventing cardiovascular diseases [35–38]. Through compounds collecting and targets screening, it turned out that HQ contained the vast majority of 20 compounds and more targets than other herbs. The analysis of the top 15 compounds with CI calculation found that HQ involved 7 effective compounds. Therefore, we could conclude that the effective compounds of SXD in the treatment of CHD were mainly contained in HQ. HQ contains astragaloside IV with significant anti-inflammatory and cardiovascular protective effects [39, 40]. For the quercetin with a high CI, it has good antithrombotic and cardiac function improvement effects, which is of great significance for the treatment of cardiovascular diseases [41]. And quercetin can reduce the levels of TNF and IL-1 β to show anti-inflammatory properties in the serum of patients with coronary artery disease [42]. Meanwhile, kaempferol can upregulate miR-26a-5p by inhibiting the TLR4/NF- κ B signaling pathway, reduce the apoptosis of endothelial cells induced by oxidized low-density lipoprotein, and play an important role in anti-atherosclerosis [43]. Formononetin, a methoxyisoflavone abundant in many herbs, has been found to alleviate atherosclerosis by modulating the interaction between KLF4 and SRA in Apo E-deficient mice [44]. Research has shown that calycosin exhibits anti-apoptotic effects by activating ER α / β and enhancing Akt phosphorylation in cardiomyocytes [45]. SM is used as the minister in SXD, and the compounds including isoferulic acid, ferulic acid and caffeic acid were the main effective compounds that can play an antioxidant role [46]. In addition to this, some other compounds have good activity in the prevention and treatment of CHD. A study by Zhang et al. luteolin has a strong cardioprotective effect, and its mechanism may be related to the down-regulation of TLR4-mediated NF- κ B/NLRP3 inflammasome *in vivo* and *in vitro* [47]. Therefore, it is speculated that SXD can treat CHD through the synergistic effect of multiple compounds.

PPI network and the published microarray data result showed that TNF, IL-6, IL-1 β , VEGFA, TP53 and PTGS2, were the core target proteins. Through cluster analysis of protein interaction network MCODE, it was found that the core target proteins were mainly concentrated in cluster 1. Cluster 1 mainly involved signaling pathways such as fluid shear stress and atherosclerosis, lipid and atherosclerosis, HIF-1 signaling pathway, IL-17 signaling pathway, TNF signaling pathway, PI3K-Akt signaling pathway, MAPK signaling pathway, etc. Cluster 2 mainly involved AGE-RAGE signaling pathway in diabetic complications, phospholipase D signaling pathway, etc. And cluster 3 mainly involved Ras signaling pathway, VEGF signaling pathway, etc. Meanwhile, these core target proteins are involved in various signaling pathways related to inflammation, apoptosis, immunity, metabolism, cell apoptosis and proliferation in the treatment of CHD. For the target with the highest degree value, TNF is an important inflammatory mediator in post-ischemic myocardial dysfunction, and the level of TNF in plasma can reflect the degree of cardiac damage in patients with CHD [48]. Similarly, IL-6 is a key cytokine, which can mediate a variety of inflammatory responses and immune regulation pathways, and it plays an indispensable role in the occurrence and development of cardiovascular diseases [49]. Besides, IL-6 is an inflammatory marker of coronary microvascular disease in women [50]. Compared with normal subjects, IL-1 β is significantly increased in patients with atherosclerosis, which plays an important role in atherosclerosis [51]. VEGFA is a major factor for promoting angiogenesis, and increased spontaneous production of VEGFA may induce angiogenesis after acute myocardial infarction, which is due to initiating ROS-ER stress-autophagy axis in the vascular endothelial cells [52,53]. TP53 is an important tumor suppressor gene and plays an important role in apoptosis, genome stability, inhibition of angiogenesis, etc [54]. The above studies showed that SXD had multi-target effects on the regulation of CHD, and these targets involved cell proliferation and apoptosis, signal transduction, inflammatory response, oxidative stress, gene expression, angiogenesis, etc. These targets were closely related to the occurrence and development of CHD, which confirmed that SXD has the effect of treating CHD.

In the process of GO enrichment analysis, BP mainly included cytokine-mediated signaling pathway, positive regulation of gene expression, negative regulation of gene expression; CC mainly involved extracellular space, and extracellular region, cell surface; MF mainly involved enzyme binding, identity protein binding, and RNA polymerase II transcription factor activity, ligand-activated sequence-specific DNA binding. From the analysis of KEGG enriched pathways, it could be seen that AGE-RAGE signaling pathway in diabetic complications, pathways in cancer, fluid shear stress and atherosclerosis, lipid and atherosclerosis, PI3K-Akt signaling pathway, MAPK signaling pathway, HIF-1 signaling pathway, EGFR tyrosine kinase inhibitor resistance. The PI3K-Akt signaling pathway is an important signaling pathway in organisms. Phosphorylated Akt can activate endothelial nitric oxide synthase and heat shock proteins to protect the myocardium [55]. Studies have found that ischemic preconditioning can activate the PI3K-Akt signaling pathway in cardiomyocytes, thereby reducing apoptosis, eliminating intracellular reactive oxygen species, and protecting mitochondrial function [56]. MAPK signaling pathway is an important intracellular transduction pathway. Studies have shown that

inhibiting MAPK signaling pathway can reduce inflammation, improve intimal thickening and inhibit plaque formation [57]. HIF-1 is a heterodimeric transcription factor composed of two subunits, HIF-1 α and HIF-1 β . HIF-1 α is highly expressed in atherosclerotic sites, and the HIF-1 signaling pathway obstruction can exert myocardial protective effect, reduce ischemia-reperfusion injury, improve cardiac function and reduce infarct size [58,59]. In addition, by regulating AGE-RAGE pathway, it can affect oxidative stress and inflammatory response in IR-induced myocardial injury in diabetic rats [60]. This is a complex process involving multiple compounds, multiple targets and multiple pathways, which reflects the holistic and systematic nature of SXD treatment of the CHD. The results of molecular docking further showed that the core targets can be stably combined with the core effective compounds in SXD, which further verified the reliability of the prediction of the network pharmacology method. For the core targets TNF, IL-6 and other core targets mentioned in this paper, we found that the gene expression of the core genes was significantly difference in circulating endothelial cells of patients with myocardial infarction [61]. Therefore, the network pharmacological results indicate that SXD may improve myocardial ischemia and reperfusion injury through inflammation and anti-apoptosis. The results of *in vivo* experiments in rats showed that SXD can significantly reduce HWI, myocardial tissue damage, serum inflammation, ALD, Ang II and NT-proBNP in rats with CHD. Therefore, the results indicated that SXD can effectively treat CHD. Based on what mentioned above, the rat cardiomyocytes H9c2 were oxygenated for 12 h after 8 h of hypoxia to establish the cell injury model of H/R, and screen whether SXD has the effect of treating myocardial damage and other injuries. The results showed that H/R could significantly inhibit the cell viability of H9c2, and different concentrations of SXD and positive drugs could improve the cell damage caused by H/R and increase the cell viability. In addition, we further explored the possible mechanism of SXD therapy. H/R can induce apoptosis of H9c2 cells, and this drug can inhibit apoptosis to a certain extent, which may be because SXD can improve cell vitality to a certain extent. Similarly, it has been reported that H/R can lead to inflammatory responses resulting from myocardial cell damage [62]. On the basis of this study, we found that SXD can inhibit the secretion of inflammatory factors in H9c2 cells and reduce the expression of inflammatory factors, and then SXD has a certain anti-inflammatory effect, so as to alleviate the secondary damage caused by the accumulation of inflammatory factors in cardiomyocytes. As shown in the review, through the predicted results of network pharmacology and experimental verification, we revealed that SXD can relieve myocardial ischemia reperfusion injury or myocardial injury caused by myocardial infarction from the perspective of anti-inflammation and anti-apoptosis. The compounds of SXD are expected to become potential drugs for the treatment of CHD, and may become the focus of future research.

5. Conclusions

In conclusion, we performed the UPLC-Q-TOF-MS/MS technology, an integrated network pharmacology and experimental verification to reveal the pharmacological mechanism of SXD against CHD. Among all effective compounds, isoferulic acid, quercetin, calycosin, ferulic acid, kaempferol, calycosin 7-O-glycoside, formononetin, astragaloside IV and saikosaponin D in SXD have high CI and good affinity with potential targets, which may play an important role in the treatment of CHD. Moreover, a further *in vivo* validation experiment that SXD alleviates myocardial tissue injury and reduce the level of serum IL-6, IL-1 β , ALD, Ang II and NT-proBNP *in vitro* validation experiment illustrated that SXD may protect myocardial cell *via* reducing the expression of the inflammatory factors and pro-apoptotic protein, thus playing a protective role in myocardial injury caused by CHD. Although the verification of the mechanism is not completely in depth, our results provide a partial research basis for the application of SXD and a new idea for the clinical prevention and treatment of myocardial injury caused by CHD.

Ethics approval and consent to participate

All procedures were strictly approved by the Animal Experiment Ethics Committee of the Shaanxi University of Chinese Medicine (Ethics Approval No. SUCMDL20220310006).

Funding

This research was funded by the National Natural Science Foundation of China (82004011 and 81903786), the Natural Science Foundation of Shaanxi Province (2022SF-221), and Subject Innovation Team of Shaanxi University of Chinese Medicine (2019-YL10).

Data availability statement

Data will be made available on request.

CRedit authorship contribution statement

Hao-ming Zhou: Writing – original draft, Software, Data curation, Conceptualization. **Shi-jun Yue:** Writing – review & editing, Funding acquisition, Conceptualization. **Wen-xiao Wang:** Methodology, Funding acquisition. **Qiao Zhang:** Investigation, Formal analysis. **Ding-qiao Xu:** Resources, Formal analysis. **Jia-jia Li:** Investigation. **Yu-ping Tang:** Funding acquisition, Conceptualization. **Xin-yu Yang:** Writing – review & editing, Funding acquisition.

Declaration of competing interest

The authors declare that they have no known competing financial interests or personal relationships that could have appeared to influence the work reported in this paper.

Abbreviation

ALD	Aldosterone
Ang II	Angiotensin II
BP	biological process
CC	cellular component
CH	roots of <i>Bupleurum chinense</i> DC
CHD	coronary heart disease
CI	contribution index
C-T-D:	compound-target-disease
DL:	drug-likeness
ECL:	chemiluminescence
GO	Gene ontology
HQ	roots of <i>Astragalus membranaceus</i> var. <i>mongholicus</i> (Bunge) Hsiao
H/R	hypoxia/reoxygenation
HWI	heart weight index
JG	roots of <i>Platycodon grandiflorum</i> (Jacq.) A. DC
KEGG	Kyoto Encyclopedia of Genes and Genomes
LAD	left anterior descending coronary artery
MF	molecular function
MI	myocardial infarction
MTT	3-(4,5)-dimethylthiazol-2-yl-2,5-diphenyltetrazolium bromide assay
NT-proBNP	N-terminal pro-brain natriuretic peptide;
OB	oral bioavailability
PPI	protein-protein interaction
PVDF	polyvinylidene difluoride;
RIPA	radio immunoprecipitation assay
ROS	reactive oxygen species
RSR	rank-sum ratio
RT-qPCR	real time quantitative PCR
SDS-PAGE	sodium dodecyl sulfate-polyacrylamide gel electrophoresis
SM	rhizomes of <i>Cimicifuga foetida</i> L
SXD	Shengxian Decoction
TCM	traditional Chinese medicine;
T-P:	target-pathway
UPLC-Q-TOF-MS/MS	ultra-performance liquid chromatography-quadrupole-time of flight-mass spectrometry
TTC	2,3,5-triphenyl-2H-tetrazolium chloride;
ZM	rhizomes of <i>Anemarrhena asphodeloides</i> Bge

Appendix A. Supplementary data

Supplementary data to this article can be found online at <https://doi.org/10.1016/j.heliyon.2024.e29558>.

References

- [1] M. Liu, Y. Wu, Role of mitophagy in coronary heart disease: targeting the mitochondrial dysfunction and inflammatory regulation, *Front Cardiovasc Med* 9 (2022) 819454.
- [2] J.E. Dalen, J.S. Alpert, R.J. Goldberg, R.S. Weinstein, The epidemic of the 20(th) Century: coronary heart disease, *Am. J. Med.* 127 (9) (2014) 807–812.
- [3] T. Doenst, A. Haverich, P. Serruys, et al., PCI and CABG for treating stable coronary artery disease: JACC review topic of the week, *J. Am. Coll. Cardiol.* 73 (8) (2019) 964–976.
- [4] C. Li, W.Y. Zhang, Y. Yu, et al., Discovery of the mechanisms and major bioactive compounds responsible for the protective effects of Gualou Kiebai Decoction on coronary heart disease by network pharmacology analysis, *Phytomedicine* 56 (2019) 261–268.
- [5] J.Y. Mao, Y.J. Wu, D.Z. Shi, Clinical application of Chinese patent medicines for treating coronary heart disease, *Zhongxiyi Jiehe Xin-naoxueguanbing Zazhi.* 19 (2021) 1409–1435.
- [6] Z. Wei, H.C. Jiao, Application advance of Shengxian Tang in the treatment of coronary heart disease, *Guoyi Luntan Zazhi* 34 (2) (2019) 64–68.

- [7] F. Zhang, Q. Zhan, X. Dong, et al., Shengxian Decoction in chronic heart failure treatment and synergistic property of Platycodonis Radix: a metabolomic approach and its application, *Mol. Biosyst.* 10 (8) (2014) 2055–2063.
- [8] G.H. Wang, F.Z. Tao, A.X. Wang, Clinical application of Shengxiantang: a review, *Zhongguo Shiyang Fangjixue Zazhi*. 27 (2021) 203–210.
- [9] J.H. Chen, Y. Lin, D.X. Wang, et al., Research progress in chemical constituents and pharmacological action of Shengxian Decoction, *Hua Xue Yu Sheng Wu Gong Cheng* 38 (4) (2021) 10–18.
- [10] F. Zhang, Q. Zhan, S. Gao, et al., Chemical profile- and pharmacokinetics-based investigation of the synergistic property of platycodonis radix in traditional Chinese medicine formula Shengxian Decoction, *J. Ethnopharmacol.* 152 (3) (2014) 497–507.
- [11] Y. Ma, B.L. Wang, L. Wang, et al., Effective components of Shengxian Decoction and its mechanism of action in treating chronic heart failure based on UHPLC-Q-TOF-MS integrated with network pharmacology, *Zhongguo Zhongyao Zazhi* 46 (10) (2021) 2489–2500.
- [12] M. Luo, Y. Hu, R. Bai, et al., Data mining-based analysis of modern Chinese medicine for the treatment of stable angina pectoris in coronary heart disease, *J. Healthc Eng* 2022 (2022) 3511974.
- [13] Z.Y. Wang, S. Li, Network pharmacology in quality control of traditional Chinese medicines, *Chin Herb Med* 14 (4) (2022) 477–478.
- [14] L.J. Zheng, Z. Zhao, D.W. Wang, et al., Network pharmacology analysis of potential mechanisms underlying the action of Radix Salviae in preventing in-stent restenosis after percutaneous coronary intervention, *J. Explor Res Pharmacol* 8 (2) (2023) 107–120.
- [15] T. Wang, X. Jiang, Y. Ruan, et al., Based on network pharmacology and in vitro experiments to prove the effective inhibition of myocardial fibrosis by Buyang Huanwu decoction, *Bioengineered* 13 (5) (2022) 13767–13783.
- [16] L.J. Chang, M.Y. Li, H.H. Wei, et al., Establishment of HPLC-ELSD characteristic fingerprints for standard decoction of Shengxian Decoction and determination of three constituents, *Zhongchengyao* 43 (8) (2021) 2010–2016.
- [17] M. Wang, H. Li, Y. Gao, et al., A multidimensional strategy to rapidly identify the chemical constituents in Shengxian Decoction by using ultra-performance liquid chromatography coupled with ion mobility spectrometry quadrupole time-of-flight mass spectrometry, *J. Sep Sci* 45 (16) (2022) 3115–3127.
- [18] J.L. Ru, P. Li, J.N. Wang, et al., TCMSP: a database of systems pharmacology for drug discovery from herbal medicines, *J. Cheminformatics* 6 (2014) 1–6.
- [19] X.Q. Shi, S.J. Yue, Y.P. Tang, et al., A network pharmacology approach to investigate the blood enriching mechanism of Danggui buxue Decoction, *J. Ethnopharmacol.* 235 (2019) 227–242.
- [20] B. Wang, Z. Wu, W. Li, et al., Insights into the molecular mechanisms of Huangqi Decoction on liver fibrosis via computational systems pharmacology approaches, *Chin. Med.* 16 (2021) 59.
- [21] T. Wang, H. Streeter, X. Wang, et al., A network pharmacology study of the multi-targeting profile of an antiarrhythmic Chinese medicine Xin Su Ning, *Front. Pharmacol.* 10 (2019) 1138.
- [22] X.Y. Yang, W.X. Wang, Y.X. Huang, et al., Network pharmacology-based dissection of the active ingredients and protective mechanism of the Salvia Miltiorrhiza and Panax Notoginseng herb pair against insulin resistance, *ACS Omega* 6 (27) (2021) 17276–17288.
- [23] Y. Wang, J. Zou, Y. Jia, et al., The mechanism of lavender essential oil in the treatment of acute colitis based on "quantity-effect" weight coefficient network pharmacology, *Front. Pharmacol.* 12 (2021) 644140.
- [24] J.X. Wang, R. Yu, W. Li, et al., Inflammatory mechanism of Yiqi Huoxue recipe with qi deficiency and blood stasis syndrome of coronary heart disease based on the theory of simultaneous treatment of heart and spleen, *Zhong Guo Shi Yan Dong Wu Xue Bao* 30 (7) (2022) 935–941.
- [25] The State Pharmacopoeia Commission of China, Pharmacopoeia of the People's Republic of China, China Pharmaceutical Science and Technology Press, Beijing, 2020.
- [26] R. Pan, Q. Zhuang, J. Wang, Ononin alleviates H₂O₂-induced cardiomyocyte apoptosis and improves cardiac function by activating the AMPK/mTOR/autophagy pathway, *Exp. Ther. Med.* 22 (5) (2021) 1307.
- [27] V.F. Salau, O.L. Erukainure, M.S. Islam, Caffeic acid protects against iron-induced cardiotoxicity by suppressing angiotensin-converting enzyme activity and modulating lipid spectrum, gluconeogenesis and nucleotide hydrolyzing enzyme activities, *Biol. Trace Elem. Res.* 199 (2021) 1052–1061.
- [28] Z. Liu, Z. Ma, H. Zhang, et al., Ferulic acid increases intestinal Lactobacillus and improves cardiac function in TAC mice, *Biomed. Pharmacother.* 120 (2019) 109482.
- [29] F. Xing, Q. Zhan, Y. He, et al., 1800MHz Microwave induces p53 and p53-mediated caspase-3 activation leading to cell apoptosis in vitro, *PLoS One* 11 (9) (2016) e0163935.
- [30] Y.S. Zhou, M.X. Zhang, Discussion on clinical application of Qixian and Shengxian Decoction in coronary heart disease, *Liaoning Zhongyi Zazhi* 43 (2016) 1873–1874.
- [31] R. Nozaki, Y.L. Hung, K. Takagi, et al., Differential protective effects of Radix astragali, herbal medicine, on immobilization-induced atrophy of slow-twitch and fast-twitch muscles, *Biomed. Res.* 41 (3) (2020) 139–148.
- [32] T. Makino, Y. Ito, S.Y. Sasaki, et al., Preventive and curative effects of Gyokuhifu-san, a formula of traditional Chinese medicine, on allergic rhinitis induced with Japanese cedar pollens in Guinea pig, *Biol. Pharm. Bull.* 27 (4) (2004) 554–558.
- [33] Z.A. Tykheev, S.V. Zhigzhitzhapova, F. Zhang, et al., Constituents of essential oil and lipid fraction from the aerial part of *Bupleurum scorzoniferifolium* Willd. (Apiaceae) from different habitats, *Molecules* 23 (6) (2018) 1496.
- [34] H. Eo, Y. Kwon, E. Huh, et al., Protective effects of DA-9805 on dopaminergic neurons against 6-hydroxydopamine-induced neurotoxicity in the models of Parkinson's disease, *Biomed. Pharmacother.* 117 (2019) 109184.
- [35] H.F. Su, S. Shaker, K. Kuang, et al., Phytochemistry and cardiovascular protective effects of Huang-qi (astragali radix), *Med. Res. Rev.* 41 (4) (2021) 1999–2038.
- [36] L.P. Yang, J.G. Shen, W.C. Xu, et al., Secondary metabolites of the genus astragalus: structure and biological-activity update, *Chem. Biodivers.* 10 (6) (2013) 1004–1054.
- [37] J. Fu, Z. Wang, L. Huang, et al., Review of the botanical characteristics, phytochemistry, and pharmacology of astragalus membranaceus (Huangqi), *Phytother Res.* 28 (9) (2014) 1275–1283.
- [38] Z. Guo, Y. Lou, M. Kong, et al., A systematic review of phytochemistry, pharmacology and pharmacokinetics on Astragali Radix: implications for Astragali Radix as a personalized medicine, *Int. J. Mol. Sci.* 20 (6) (2019) 1463.
- [39] L. Li, X. Hou, R. Xu, et al., Research review on the pharmacological effects of astragaloside IV, *Fundam. Clin. Pharmacol.* 31 (1) (2017) 17–36.
- [40] G. Gong, H. Yu, Y. Zheng, et al., Astragaloside IV, a saponin from *astragalus membranaceus* var. *mongolicus*, induces expressions of heme recycle proteins via signaling of Nrf2/ARE in cultured macrophages, *J. Ethnopharmacol.* 265 (2021) 113389.
- [41] T.W. Oh, H.J. Do, J.H. Jeon, et al., Quercitrin inhibits platelet activation in arterial thrombosis, *Phytomedicine* 80 (2021) 153363.
- [42] N. Chekalina, Y. Burmak, Y. Petrov, et al., Quercetin reduces the transcriptional activity of NF- κ B in stable coronary artery disease, *Indian Heart J.* 70 (5) (2018) 593–597.
- [43] X. Zhong, L. Zhang, Y. Li, et al., Kaempferol alleviates ox-LDL-induced apoptosis by up-regulation of miR-26a-5p via inhibiting TLR4/NF-kappaB pathway in human endothelial cells, *Biomed. Pharmacother.* 108 (2018) 1783–1789.
- [44] C. Ma, R. Xia, S. Yang, et al., Formononetin attenuates atherosclerosis via regulating interaction between KLF4 and SRA in apoE (-/-) mice, *Theranostics* 10 (3) (2020) 1090–1106.
- [45] B. Liu, J. Zhang, W. Liu, et al., Calycosin inhibits oxidative stress-induced cardiomyocyte apoptosis via activating estrogen receptor- α/β , *Bioorg. Med. Chem. Lett* 26 (1) (2015) 181–185.
- [46] X.C. Li, J. Lin, Y.X. Gao, et al., Antioxidant activity and mechanism of rhizoma cimicifugae, *Chem. Cent. J.* 6 (2012) 1–10.
- [47] X. Zhang, Q. Du, Y. Yang, et al., The protective effect of luteolin on myocardial ischemia/reperfusion (I/R) injury through TLR4/NF-kappaB/NLRP3 inflammasome pathway, *Biomed. Pharmacother.* 91 (2017) 1042–1052.
- [48] K. Safranow, V. Dziedziejko, R. Rzeuski, et al., Plasma concentrations of TNF-alpha and its soluble receptors sTNFR1 and sTNFR2 in patients with coronary artery disease, *Tissue Antigens* 74 (5) (2009) 386–392.
- [49] A. Ali, M. Boutdir, A.S. Aromolaran, Cardiotoxicity, inflammation, and arrhythmias: role for interleukin-6 molecular mechanisms, *Front. Physiol.* 9 (2019) 1866.

- [50] D. Gurzau, A. Sitar-Taut, B. Caloian, et al., The role of IL-6 and ET-1 in the diagnosis of coronary microvascular disease in women, *J. Personalized Med.* 11 (2021) 965.
- [51] W. Mai, Y. Liao, Targeting IL-1 β in the treatment of atherosclerosis, *Front. Immunol.* 11 (2020) 589654.
- [52] J. Zou, Q. Fei, H. Xiao, et al., VEGF-A promotes angiogenesis after acute myocardial infarction through increasing ROS production and enhancing ER stress-mediated autophagy, *J. Cell. Physiol.* 234 (10) (2019) 17690–17703.
- [53] L. Zentilin, U. Puligadda, V. Lionetti, et al., Cardiomyocyte VEGFR-1 activation by VEGF-B induces compensatory hypertrophy and preserves cardiac function after myocardial infarction, *Faseb. J.* 24 (5) (2010) 1467–1478.
- [54] Y. Dong, H. Chen, J. Gao, et al., Molecular machinery and interplay of apoptosis and autophagy in coronary heart disease, *J. Mol. Cell. Cardiol.* 136 (2019) 27–41.
- [55] C. Lu, X. Wang, T. Ha, et al., Attenuation of cardiac dysfunction and remodeling of myocardial infarction by microRNA-130a are mediated by suppression of PTEN and activation of PI3K dependent signaling, *J. Mol. Cell. Cardiol.* 89 (2015) 87–97.
- [56] L. Zhao, X.R. Yang, X. Han, MicroRNA-146b induces the PI3K/Akt/NF- κ B signaling pathway to reduce vascular inflammation and apoptosis in myocardial infarction by targeting PTEN, *Exp. Ther. Med.* 17 (2) (2019) 1171–1181.
- [57] S.S. Li, H.H. Yu, W.Y. Tian, Research progress of effect of traditional Chinese medicine in prevention and treatment of atherosclerosis based on signal pathway related to inflammatory response, *Zhongguo Shiyan Fangjixue Zazhi* 26 (2020) 180–186.
- [58] G.L. Wang, B.H. Jiang, E.A. Rue, et al., Hypoxia-inducible factor 1 is a basic-helix-loop-helix-PAS heterodimer regulated by cellular O₂ tension, *Proc. Natl. Acad. Sci. U.S.A.* 92 (1995) 5510–5514.
- [59] T. Heriansyah, N. Nafisatuzzamrudah, F.N. Aini, et al., Reduction in vasa vasorum angiogenesis by Lp-PLA2 selective inhibitor through the HIF-1 α and VEGF expression under dyslipidemic conditions in atherosclerosis pathogenesis, *Cardiovasc. Hematol. Agents Med. Chem.* 16 (2) (2018) 114–119.
- [60] K. Suchal, S. Malik, S.I. Khan, et al., Protective effect of mangiferin on myocardial ischemia-reperfusion injury in streptozotocin-induced diabetic rats: role of AGE-RAGE/MAPK pathways, *Sci. Rep.* 7 (1) (2017) 42027.
- [61] E.D. Muse, E.R. Kramer, H. Wang, et al., A whole blood molecular signature for acute myocardial infarction, *Sci. Rep.* 7 (1) (2017) 12268.
- [62] X. Hu, R. Ma, J.L. Cao, et al., CircSAMD4A aggravates H/R-induced cardiomyocyte apoptosis and inflammatory response by sponging miR-138-5p, *J. Cell Mol. Med.* 26 (6) (2022) 1776–1784.